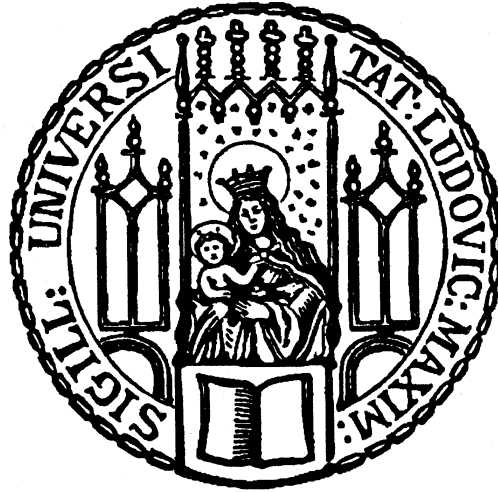**Aus der Klinik und Poliklinik für Psychiatrie und Psychotherapie der Ludwig-Maximilians-Universität München**

Universität München Director: Prof. Dr. med. Peter Falkai

Univariate and multivariate pattern analysis of preterm subjects: a multimodal neuroimaging study

Dissertation
zum Erwerb des Doktorgrades der Humanbiologie
an der Medizinischen Fakultät der
Ludwig-Maximilians-Universität München

vorgelegt von
Jing Shang
aus Jiangsu, China
2019

Mit Genehmigung der Medizinischen Fakultät
der Ludwig-Maximilians-Universität München

Berichterstatter : Prof. Dr. med. Nikolaos Koutsouleris

Promovierter Mitbetreuer: Dr. Dominic Dwyer

Mitberichterstatter : Priv. Doz. Dr. Arthur Liesz

Dekan : Prof. Dr. med. dent. Reinhard Hickel

Tag der mündlichen Prüfung : 26.06.2019

To myself

"One small crack does not mean that you are broken, it means that you were put to the test and you didn't fall apart."

— Linda Poindexter

"Despite knowing the journey and where it leads, I embrace it and welcome every moment."

— Ted Chiang, Story of Your Life

TABLE OF CONTENTS

Declaration

I hereby declare that all of the present work embodied in this thesis was carried out by me from 12/2014 until 02/2019 under the supervision of Prof. Dr. med. Nikolaos Koutsouleris and Dr. Dominic Dwyer, Klinik Für Psychiatrie und Psychotherapie der Ludwig-Maximilians-Universität München; and PD. Dr. med. Christian Sorg, Department of Psychiatry, Klinikum rechts der Isar and Department of Neuroradiology, Technische Universität München. This work has not been submitted in part or full to any other university or institute for any degree or diploma.

Part of the work was done by others, as mentioned below:

1. Dr. Josef Bäuml, post-doctoral fellow, Technische Universität München, Germany. He works as a major group member of Bavarian Longitudinal Study (BLS) in Munich, and has performed the data collection. The data description is presented in the materials and methods part , section 3.1 of this thesis.

Part of the work has been published in Human Brain Mapping (Sep 12th, 2018).

Date: Feb. 12th, 2019   Signature: ………………….

Place: Munich, Germany   (Jing Shang)

ZUSAMMENFASSUNG

In zahlreichen Studien wurden bei Frühgeborenen ausgedehnte und langfristige Veränderungen der funktionellen Konnektivität und der Volumina in kortikalen und subkortikalen Gehirnregionen untersucht. Jedoch bleibt die Beziehung zwischen den regionalen Veränderungen der spontanen BOLD-Fluktuationen und den Volumina in der grauen Substanz unklar, wie z.B. im lateralen Temporalkortex. Außerdem bleibt offen, ob Klassifizierungsmethoden basierend auf MRT-Daten erfolgreich angewendet werden können, um Frühgeborene zu identifizieren. In der vorliegenden Doktorarbeit stellte ich die Hypothesen auf, dass bei Frühgeborenen 1. die neuronale Erregbarkeit und Hirnaktivität, gemessen via funktioneller Konnektivität und Ruhe-fMRT, mit veränderten niederfrequenten Schwankungen und neonatalen Komplikationen assoziier ist; dass 2. veränderte regionale funktionelle Konnektivität mit reduzierten Gehirnvolumina überlappt; und dass 3. multivariate neuroanatomische und funktionelle Gehirnmuster als Merkmale verwendet werden können, um Frühgeborene von Reifgeborenen zu unterscheiden. Um diese Hypothesen zu untersuchen, wurden bei 94 sehr früh und/oder sehr unreif geborenen und 92 reifgeborenen Erwachsene strukturelle Veränderungen mittels voxelbasierter Morphometrie (VBM) gemessen, während die Ruhe-fMRT Ergebnisse für die Schätzung der niederfrequenten Amplituden (ALFF) verwendet wurden. Die Ergebnisse stützen die Hypothesen, indem sie in den univariaten Analysen zeigen, dass die ALFF in den linken lateralen Temporalkortex Regionen reduziert waren und zwar unabhängig davon ob für

ZUSAMMENFASSUNG

das globale Signal kontrolliert wurde oder nicht. Außerdem waren diese Verringerungen mit neonatalen Komplikationen und kognitiven Leistungen assoziiert. Zweitens überlappten in den linken lateralen Temporalkortex Regionen verringerte ALFF und VBM Werte. In den multimodalen und multivariaten Mustererkennungsanalysen (MVPA) erzielte der Klassifikator der grauen Substanz (GMV) eine höhere Genauigkeit (80.7%) als der ALFF Klassifikator (77.4%). Die späte Fusion von GMV und ALFF erzielte keine höhere Genauigkeit (80.4%) als die singulären Klassifikationen. Moderator Analysen ergaben, dass die Neuro-Frühgeburtlichkeits-Leistung vorzugsweise von neonatalen Komplikationen bestimmt war. Zusammengefasst zeigen diese Ergebnisse den langfristigen Effekt einer Frühgeburt auf die strukturelle und funktionelle Organisation der lateralen Temporalkortex Regionen. Diese Arbeit zeigt weiterhin, dass multivariate Mustererkennungsanalysen, wie „support vector machine" (SVM) MRT-basierte Biomarker darstellen könnten und Frühgeborene reliabel erkennen können.

Summary

Widespread lasting functional connectivity (FC) and brain volume changes in cortices and subcortices after premature birth have been researched in recent studies. However, the relationship remains unclear between spontaneously slow blood oxygen dependent level (BOLD) fluctuations and gray matter volume (GMV) changes in specific brain areas, such as temporal insular cortices, and whether classification methods based on MRI could be successfully applied to the identification of preterm individuals. In this thesis I hypothesized that in prematurely born adults 1. Ongoing neural excitability and brain activity, as estimated by regional functional connectivity of resting-state functional MRI (rs-fMRI) is accompanied with altered low-frequency fluctuations and neonatal complications; 2. Altered regional functional connectivity is connected with superimposed cerebral structural reductions; and 3. multivariate neuroanatomical and functional brain patterns could be treated as features to identify preterm subjects from term subjects individually. To investigate these hypotheses, the principal results of structural alterations were measured with voxel-based morphometry (VBM), while rs-fMRI outcomes were estimated with amplitude of low-frequency fluctuations (ALFF) in analysis with ninety-four very preterm/very low birth weight (VP/VLBW) and ninety-two full-term (FT) born young adults. The results of the thesis support the hypotheses by showing that, in univariate results, first in VP/VLBW grownups, ALFF was decreased in the left lateral temporal cortices no matter with global signal regression, and this reduction was closely associated with neonatal complications and cognitive variables. Second overlapped brain

regions were found between reduced ALFF and reduced brain volumes in the left temporal cortices, and positively associated with each other, demonstrating a potential relationship between VBM and ALFF in this brain area. In multimodal multivariate pattern recognition analysis (MVPA), the gray matter volume (GMV) classifier displayed a higher accuracy (80.7%) contrast with the ALFF classifier (77.4%). The late fusion of GMV and ALFF did not outperform single GMV modality classification by reaching 80.4% accuracy. Moderator analysis from both rs-fMRI and structural MRI (sMRI) uncovered that the neuro-prematurity performance was predominantly determined by neonatal complications. In conclusion, these outcomes exhibit the long term effects of premature labour on lateral temporal cortices, which changed in both ongoing BOLD fluctuations and decreased cerebral structural volumes. This thesis further provided evidence that multivariate pattern analysis such as support vector machine (SVM) may identify imaging-based biomarkers and reliably detect signatures of preterm birth.

1. Introduction

1.1 Definition of preterm

Premature birth, i.e., neonatal born before 37 weeks of gestation or in low birth weight under 2500g, has a global prevalence of over 10% [1,2]. It leads newborns to take on more risks to suffer from birth complications, disadvantageous effects of clinical brain development and functionality in the future, including cognitive, behavioral and attentional socialization deficits [2,3]. Especially, premature born people are more easily subjected to chronic neurocognitive impairments, neurological and mental disorders, since neural migration and cortical folding are happening between the 24th and 32nd gestational week in utero period [4,5]. Another point of view defined prematurity reference to people born with low birth weight as well since the vast majority of infants born preterm are along with a low birth weight [6]. Taking the gravity of neurodevelopment of early fetus into consideration, danger for detrimental effects goes up appreciably with quite premature born people, i.e., born very preterm (VP; gestational age < 32 weeks) and/or with very low birth weight (VLBW; < 1500 g) [5,7].

1.2 Epidemiology of preterm birth

Spontaneous preterm labour, infectious delivery, and premature rupture of the membranes are significant top three causes of spontaneous perinatal morbidity and mortality in developed nations [8]. The common reasons initiated by the preterm labour usually includes fetal inflammatory, vascular disease, uterine overdistension and so on [8,9]. Among these risk factors of preterm

delivery, cervical shortening, increased cervical-vaginal fetal fibronectin concentration and bacterial vaginosis are the most potent predictors [8]. Except for the above multiple factors which may trigger or exacerbate preterm birth, other pathophysiological elements such as genetics, epigenetics, socio-economic status of parents, and maternal-fetal factors are vital to preterm infants [10].

Although survival rates have significantly improved lately for babies born prematurely, mortality and sequelae cannot be ignored. Bronchopulmonary dysplasia and encephalopathy of prematurity occurred most frequently [11], which contributes to elevated rates of chronic neurological and health issues [11,12]. Short-term sequelae of premature neurodevelopment incorporate periventricular leukomalacia (PVL), periventricular hemorrhagic infarction (PHI), cerebral paralysis and germinal matrix hemorrhage intraventricular hemorrhage (GMH-IVH), while long-term complications of premature neurodevelopment include intellectual, behavioral, attentional and social shortages [7].

1.3 Pathophysiology of premature brain changes

The greater danger of detrimental neurocognitive results is closely correlated with more impaired brain maturation procedure [10,13]. Brain maturation abnormalities relative with preterm birth is generally triggered by detrimental prenatal and perinatal events like cerebral lesion due to hypoxia-ischemia, cerebral hemorrhage, along with other infections in addition to infant stress [2].

Introduction

In the microscopic level, the procedures of brain injury mostly impair the progression of pre-myelinating oligodendrocytes, neurotransmitter gamma-aminobutyric acid (GABA)-ergic interneurons, and subplate neurons. These cell types play fundamental roles in the creation of cortical tissue, cerebral structure (including gray matter and white matter), along with anatomical connectivity [14-19]. For instance, during 15-35 gestational weeks, the thalamocortical axon, basal forebrain cholinergic, and cortico-cortical afferents growing into inner zone of cortical plate and are regulated by different populations of subplate neurons [20]. These whole processes tend to be impaired in prematurity because the subplate neurons are vulnerable to perinatal hypoxia and ischemia [2], further leading to decreased subplate neuron arborization and regional microcircuit development [21].

In the macroscopic level, decreased deep white matter volume, e.g. the corpus callosum was mostly found in diffusion tensor imaging (DTI) studies, as described in preterm children [22-25], adolescents [26-29] and adults [30-33]. Likewise reduced gray matter volume concentrate insistently on chosen subcortical, e.g., thalamus, striatum, as well as cortical areas, for instance, the medial and lateral temporal cortices [34-39].

Recent research suggests that the resting-state functional resonance imaging (rs-fMRI) analysis demonstrates spontaneous low-frequency (<0.1 Hz) neuronal oscillations [40,41]. This spatiotemporal signal indirectly measured with functional connectivity, reflects ongoing neural excitability and activity in slow fluctuation, together with intracellular descriptions in animal studies, by showing that resting-state oscillations and hemodynamics are modulated by

the increase in blood flow combined with spontaneous and synchronized neural activity [42-45]. These macroscopic signals signify a sort of basic default cortical network activity generated by fundamental neuronal microcircuits, such as single neuron and synaptic reverberation of the spiking activity [46].

1.4 Long-term effects on premature brain changes

Due to limited human autopsy brain research [47], and the fact that the value of the tissue may change broadly relying upon postmortem interval as well as the modes of tissue preservation, neuroimaging studies may work as a good alternative, which permits for a substantial number of population sampling but without traumatic examination.

Slow oscillations, treated as the spontaneously default activity of the cortical network [46], measured by intrinsic functional connectivity of rs-fMRI, have aroused increasing interest in preterm research. For example, newborn brain development was explored using rs-fMRI from low frequency [48-50] to high frequency [51], with proof that network connections are disrupted in either the short term [52] or long term functional connectivity [53] in premature newborns. For some research based on preterm children and adolescents, no significant differences or subtle alterations in functional connectivity were demonstrated between preterm and term groups [53-55]. Contrastingly, some other resting-state research focus on preterm adolescents and adults manifested that alterations in executive function along with executive control networks [56], visual and attention relevant intrinsic networks [57], the basal ganglia-, thalamus-, and salience network [58] when compared to term controls. Prematurely born children and adolescents are at high risk for language

deficits especially at school age, but the neurobiological basis of these findings have been less well studied than other high order cognitive functions. Wilke and his colleagues proved injury of functional connectivity between interhemispheric superior temporal lobe (STL) language regions in preceding early preterm born children and teenagers, with task-based and non-task-based brain functional connectivity analyses [59]. Similarly, rs- functional connectivity in the left cerebral areas, related with semantic language areas, indicates differences in young adults born prematurely compared to healthy term control subjects [60,61]. On the contrary, Scheinost and his colleagues showed preterm young adulthood participants exhibited a significant decrease in right hemisphere lateralization correlate with language scores [62].

Cellular immaturity in the gray and white matter might interrupt a vital development with fast cerebral growth concurrently, and increased neuronal connectivity linked to the elaboration of the dendritic differentiation, axonal arbor, synaptogenesis and myelination [63]. Previous evidence observed that volumetric grey matter differences widely extended between very preterm individuals and full term peers in adolescence [38] and this alteration mainly continue to adulthood [64]. Longitudinal investigation from youth (15 years) to adults (19 years) discovered decreased GM volume in the cerebellum, subcortex, parietal and occipital cortex, furthermore the smaller these brain regions the higher rates of psychiatric symptoms of the VLBW group [65,66]. Therefore it was concluded that considerably smaller subcortical and cerebellar GM volumes in VLBW individuals might indicate a threat for developing and maintaining psychiatric disorders through their teenage years [65,66]. Some studies contributed extensive gray matter abnormalities partially to

atypical brain development of prematurity instead of perinatal brain injuries. For example, Karolis, et al. found that adolescents and adults born very prematurely had older brains than counterparts by revealing decreased global and modular GMV patterns related to the procedures for accelerated brain maturation [36]. However, in a recent MRI meta-analysis, no significant maturational differences are discovered for either GM or WM volumes between preterm-born and term-born peers from childhood to adolescence [67]. According to the concept of an 'encephalopathy of prematurity' raised by Volpe [2], the impaired constellation of structural abnormality of preterm survivors may be due to both disruptive consequence and developmental trajectories.

Diffusion tensor imaging (DTI) as a popular MRI technique, quantifies fiber orientation and the diffusion of water within white matter tissues, has been recently used to study the structural basis of white matter development in the preterm brain. Fractional anisotropy (FA), as the most commonly used DTI parameter, has been widely used to assess white matter microstructural abnormalities and integrity of white matter pathways [68]. Widespread white matter tracts of reduced FA are found in the uncinate fasciculus of preterm children [24], the internal capsule and superior fasciculus of adolescents [28,29] and the superior longitudinal fasciculus of adults [30,31,37]. Preterm infants at term-equivalent age exhibited most consistently abnormalities in FA of the corpus callosum [68]. The corpus callosum connects the left and right cerebral hemispheres, and is probably involved in motor, perceptual, and cognitive functions [69,70]. It increases in size when it reaches its peak in young adulthood, then slightly declines into old age [71]. Since FA is sensitive to the alignment of

white matter fibers and structural integrity [72], it suggests that reduced FA in the corpus callosum may be caused by disorganization of white matter fibers [28,73,74] or impaired myelin and/or poorer packing of axons [30].

1.5 The relationship between rs-fMRI and sMRI in prematurely born subjects

Intrinsic functional connectivity is changed in the lateral temporal cortices and subcortex such as striatum, thalamus, and these rs-fMRI signals are overlapped with relevant GMV loss [58]. The connection between neuronal oscillations in cortical networks coupling with underlying brain volume changes after premature birth implies possible alterations in basic, slow spontaneously ongoing neural activity especially in regions of constant brain volume reduction, possibly as a result of prematurity-induced brain microstructure changes [75]. The point was further supported by revealing variability in the amplitude of low frequency fluctuations (ALFF), an indirect indicator for regional functional connectivity in the resting brain, coincided with anatomic areas changes in 1414 healthy subjects [76]. The overlapping structural and functional brain changes in the subcortex, such as hippocampal and striatal volume which correlated with dopamine synthesis was found in prematurely born individuals by F-Dopa-PET [77]. Another study using DTI and task fMRI also confirmed the essential role of subcortical areas in prematurity by showing the overlapped region between white fibers and brain activity in thalamo-cortical radiations of preterm newborns [78]. But it should be noted that variability of structural and functional connectivity is not entirely coupled [76],

which implies that brain structural and functional connection does not necessitate with each other.

1.6 Definition of ALFF and VBM

Amplitude of Low-Frequency Fluctuations (ALFF), an alternative neuroimaging method to quantify fundamental features of rs-fMRI, is explained as spontaneous fluctuations in BOLD-fMRI signal strength for a given region in the resting brain. For every voxel, ALFF measures the magnitude of the fluctuation of the voxel. It has been suggested that ALFF reflects the local properties of BOLD signal fulctuations in the resting state [79-81], and is calculated as standard deviation of the low frequency time series (usually 0.01-0.1 Hz) [82,83]. ALFF, investigating the synchronicity of spontaneous oscillations across the whole brain, is assumed to indirectly reflect slow wave neuronal activity and excitability in specific frequency [42-44,46,76,79,84,85]. In detail, regional cortical microcircuits generate slow oscillations spontaneously between the periods of intense activity (i.e., up-state) and silence (i.e., down-state) at frequencies below 1Hz restricted to the cortices [46,86]. Recent event-related task research supplied tight correspondence between BOLD signals and electrophysiological signals by using simultaneous neuronal imaging and optical recordings of local neurons in animals, which revealed that blood oxygenation fluctuations resulting from slow oscillations in neuronal firing and excitability [42,85,86] and their coupling [43,44].

Voxel-based morphometry (VBM) is a morphometric measurement which includes a comparison of the local concentration of gray matter on a voxel-by-

voxel basis [87]. As a completely automated whole brain procedure, this facilitates not only the evaluation of separate brain compartments, namely gray matter, white matter, cerebrospinal fluid (CSF) and total intracranial volume (TIV) with some degree of accuracy, but also subregions within these compartments.

1.7 Machine learning and preterm birth

Machine learning is the study making use of algorithms to build mathematical models based on training samples, then make predictions or decisions that reach an optimal solution to a problem. The integration between machine learning approach and medical imaging have been recently studied and tested in different clinical fields. In comparison with conventional univariate analysis methods, such as statistical tests that are conducted on each voxel independently, in order to make inferences regarding effects of interest in a group-level, multi-voxel (or multivariate) pattern analysis (MVPA) methods have some empirically verifiable advantages over univariate approaches: first, MVPA are more appropriate for high-dimensional neuroimaging data by examining multiple voxels jointly; second, MVPA could forecast outcomes from separate data on the grounds of previously identified brain-behavioral connections; third, MVPA is utilized to recognize patterns of distinction between the classes and make an inference based on a single-subject level instead of a group level.

There are two crucial and major methodological approaches in MVPA: supervised and unsupervised machine learning techniques. Classification and regression will be utilized in this thesis, which are the most two frequently

used supervised learning methods, when the variables are predicted discrete or continuous [88]. The purpose of a SVM classifier is to locate a decision boundary in 2D space or decision surface in hyperplane, which is affected by support vectors. Then SVM builds a training model that might optimally differentiate between classes with maximized empirical margin. Finally based on that boundary/surface assign new, previously unknown data into the categories to test the training algorithm. The SVM algorithm is decided by support vectors, which are cases on the closest external borders of the distributions. This advanced technique has been applied to the MRI database (the values of observed features, e.g. voxels) in which a classifier is trained to discriminate between different brain states (e.g. disease state) and then predict the brain states in a new set of MRI data. These neuroimage features are usually extracted from the patterns of gray or white matter volume or brain activation across the whole brain. In this module, I used linear classifiers, which can discern the contribution of voxel (x) to detecting category (y) by looking at the weight (w) between voxel (x) and category (y). In more details, feature selection as the first step, involves deciding which voxels of MRI data will be included in the classification analysis and treated as identified features (x) (Figure 1a). The next step, called pattern assembly, involves sorting the voxels contributing to prematurity. These discrete 'brain patterns' are labeled as VP/VLBW or FT corresponding to the pattern of functional connectivity or morphological changes across the selected brain voxels (Figure 1b). The weights of voxels are driven by the classification and plotted as a weight map (w) across brain regions. The different colors indicate the weights of the classifier. Different classifiers may provide various brain maps contributing to

different sensitive features and algorithm design. At last, the classifier weights can be mapped onto the new brain activation/structural maps to quantify the degree to which the pattern responds to particular brain states (Figure 1c).
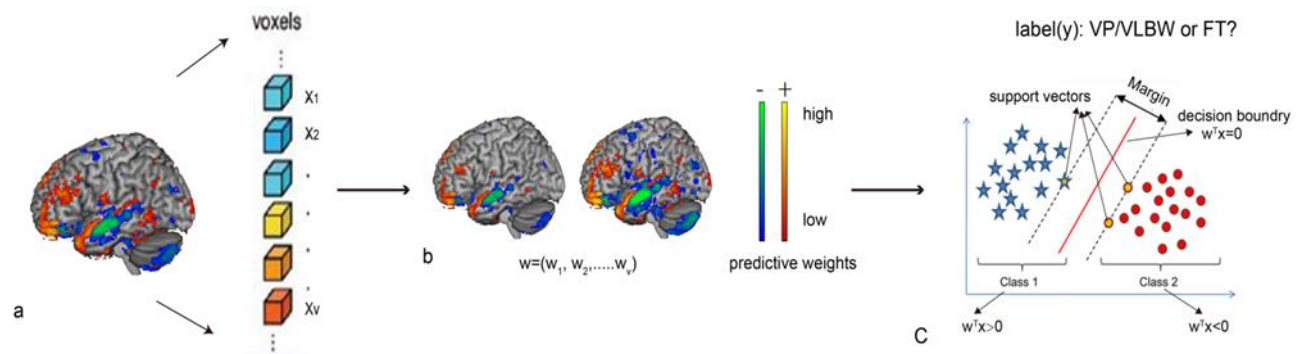
Figure 1*. Explanation of support vector classification with neuroimage data.*

A) Feature extraction including converting three-dimensional images to a column vector (x_1, x_2, ….x_v) of features with each value corresponding to the intensity of an individual corresponding voxel. B) Predictive brain models tightly coupled with target outcomes. w_1, w_2, … w_n represent predictive weights across voxels which contain helpful discriminative information. C) Discrimination between classes according to neuroimage features. Abbreviations: FT, full-term; VP/VLBW, very preterm/very low birth weight.

Support vector regression (SVR) is another type of supervised MVPA, and it is a set of statistical processes to explore the relationships among independent variables and continuous dependent variables by providing the optimum fit between them, while demonstrating a margin within certain threshold of reliable generalization and minimizing the generalization error boundary.

Recently, multivariate machine learning techniques have manifested the feasibility to diagnose neuropsychiatric illnesses and predict illness onset in

ultra-high risk psychosis [89,90], schizophrenia [91-96] and Alzheimer's [97,98]

individuals using resting-state or structural MRI data. In the preterm research

field, only a few MVPA studies have worked on prematurely born infants'

brains using functional connectivity, confirming the method was able to

discriminate subjects solely based on functional connectivity, and predict

maturity or characterize brain alterations [99,100]. SVR is able to quantify

estimation of birth gestational age in preterm individuals using term equivalent

(38-40 weeks) rs-fMRI data [99]. Brain-based age (BrainAGE) prediction is a

recently popular method utilizing SVR. Its intentions are to gauge a person's

age and individual brain maturation according to brain data obtained from

magnetic resonance imaging. The BrainAGE framework based on MRI is well-

validated to predict individual brain cognitive impairments [101], traumatic brain

injury [102] and schizophrenia [103], and found these patients' brains were

estimated to be older than their chronological age. The BrainAGE framework

is also successfully applied to preterm-born children, adolescents and adults,

results in a significantly lower estimated brain age than chronological age in

prematurely born subjects [36,104]. The above findings imply that MVPA may

offer an option to predict neurodevelopmental outcome in individuals, and

demonstrate its successful clinical application in preterm studies.

2. Hypotheses, Aim and Plan

Considering the mixed neuroimage results of prematurely born individuals from different age periods, and these very preterm born subjects more easily encounter critical problems in their childhood and later life: in addition to neurological and neuropsychological disorders, social competence and behavioral impairments in school are worth of attention [105]. Therefore, it is necessary to work on a large sample of grownups who were born at or before 32 weeks or a low birth weight (<1500 g) with rs-fMRI and structural MRI data to investigate long term brain changes in regional functional connectivity and gray matter.

My hypotheses are : 1. Oscillations in ongoing neural excitability and activity, as measured by regional rs-fMRI, are consistently changed in prematurely born adults, accompanied with significant brain volume alterations; 2. Preterm birth results in superimposed specific alterations in both regional functional connectivity and gray matter volume, and it remains in the adulthood; 3. Neuroimaging-based MVPA such as the SVM may reliably detect the signature of preterm individuals, therefore MVPA is essential for group and individualized categorization; 4. Sociodemographic, neonatal complications and cognitive moderators may determine the neurodevelopment outcome.

To the best of my knowledge, no study has investigated VP/VLBW adulthood brains using univariate and multivariate in multi-modal analysis. The aim and plans of this study are

Hypotheses, Aim and Plan

1.In the univariate analysis, I tested the group difference between VP/VLBW and FT by ALFF and VBM, and whether group impacts on ALFF proved indeed associated with gray matter, degree of prematurity and adult neurocognitive performance. This assumption was performed by two-sample t-tests in two modalities. Partial correlation analyses were conducted between ALFF values and VBM values, prematurity relative scores and IQ scores in the VP/VLBW group controlling for variables of no interest.

2. In the MVPA I attempted to validate and expand upon these group findings to the individual level, together with the coherence in the temporal and subcortical changes in two modalities. Moreover, patterns of feature weights illustrating the scope and scale of the consequences of prematurity. Then sociodemographic, neonatal complications and neurocognitive data were evaluated to explore predictive biomarkers across the preterm adulthood individuals using support vector regression, quantify the importance of clinical features on the brain decision scores individually, then confirm their relationship using the Spearman univariate model.

3. Material and Methods

3.1 Participants

Recruitment of participants belongs to prospective Bavarian Longitudinal Study (BLS) [106,107]. This geographically characterized study selects neonatal infants born at prematurely risk in South Bavaria, Germany. Of the preliminary 682 infants born VP/VLBW, 411 newborns were qualified for the 26-year follow-up evaluation, and 260 (63.3%) engaged in psychological examinations [108]. Of the initial 916 term-born control infants from the same obstetric hospitals, 350 were randomly chosen as term controls within the matched society categorization, e.g. sex and family socioeconomic status, in order to compare with the VP/VLBW sample. Of them, 308 were eligible for the 26-year longitudinal tracking assessment, and 229 (74.4%) engaged in psychological tests. Of the sample evaluated in adulthood, 101 VP/VLBW as well as 102 FT individuals were scanned using 3.0T MRI at 26 years. MRI assessments were completed at two different locations: the Department of Neuroradiology, Klinikum Rechts der Isar, Technische Universität München, Germany (N = 138), and the Department of Radiology, University Hospital Bonn, Germany (N = 67). The research was authorized by the local ethics committees of the Klinikum Rechts der Isar and University Hospital Bonn. All study participants gave written informed consent and received travel expenses and payment for attendance. A comprehensive description of participants, especially including MRI-based brain abnormalities showed as below.

Material and Methods

Table 1. Description of participants: MRI-based brain abnormalities

	VP/VLBW	FT
Cysts	1	1
T2 hyperintensity	4	1
Meningioma (left occipital)	-	1
Polymicrogyria	1	-
Ventriculomegaly	3	-
Focal dysplasia (corpus callosum)	1	-
Total	10	3

3.2 Birth-related variables

Gestational age (GA) was calculated from maternal reports on the first day of the last menstrual period and sequential ultrasounds during pregnancy. Clinical assessment at birth with the Dubowitz method was implemented [109], in cases the two measurements differed by more than 2 weeks gap. Birth weight (BW), and Intensity of Neonatal Treatment Index (INTI), standardized optimality scores for neonatal complications (OPTI) [110], duration of Neonatal Treatment Index (DNTI), which signify the period and intensity of medical treatment after birth. Along with maternal age and family socioeconomic status (SES) at birth, were recorded from obstetric documentary [106,111].

3.3 Cognitive assessments

The neurocognitive performance was evaluated by independent trained psychologists using the Wechsler Adult Intelligence Scale (WAIS III) in

Material and Methods

German version [112], then converted to age-normed verbal IQ, performance IQ, and Full-Scale IQ scores at the average age of 26 years.

3.4 Image Acquisition

At both Munich and Bonn sites, MRI data was originally collected on Philips Achieva 3T TX systems (Achieva, Philips, the Netherlands), using an 8-channel SENSE head coil. As a result of a scanner upgrade, data acquisition in Bonn had to convert to Philips Ingenia 3T system with an 8-channel SENSE head coil after 17 participants receiving scanning. After N = 133 participants, data acquisition in Munich switched to the same Philips Ingenia 3T version as in Bonn. To account for potential confounds introduced with scanner variations, data analyses included scanner identities as covariates of no interest. Across all scanners, sequence parameters were kept uniform. Scanners were assessed regularly to meet optimal scanning requirements. MRI physicists at the University Hospital Bonn and Klinikum rechts der Isar regularly scanned imaging phantoms, to guarantee within-scanner signal consistency with the passage of time. Signal-to-noise ratio (SNR) was not substantially different between scanners (one-way ANOVA with variable "scanner-ID" [Bonn 1, Bonn 2, Munich 1, Munich 2]; $F(3,182) = 1.84$, $p = 0.11$).

Resting-state fMRI data were gathered for 10 min 52 s from a echo-planar sequence (TE = 35 ms, TR = 2608 ms, flip angle = 90°, FOV = 230 mm², matrix size = 64 × 63, 41 slices, thickness 3.58 and 0 mm interslice gap, reconstructed voxel size = 3.59 × 3.59 × 3.59 mm³) leading to 250 volumes of BOLD fMRI data every single subject. Afterward, a high-resolution T1-

weighted 3D-MPRAGE sequences were also collected for each subject using the following parameters: TI = 1300 ms, TR = 7.7 ms, TE = 3.9 ms, flip angle = 15°; 180 sagittal slices, FOV = 256 × 256 × 180 mm, reconstruction matrix = 256 × 256; reconstructed voxel size = 1 × 1 × 1 mm³. Prior to undergoing the resting-state sequence instantly, participants were guided to close their eyes during rs-fMRI scanning but refrain from falling asleep. MRI technicians confirmed that subjects remained awake by interrogating via intercom instantaneously following the rs-fMRI scan.

3.5 Data preprocessing

SPM12 (http://www.fil.ion.ucl.ac.uk/spm) along with DPARSF [113] are basically used for preprocessing. For every subject, functional volumes were firstly realigned to the first image of the time series to correct for head movement, then coregistered to each same subject's high-resolution structural T1 image. Afterward, each T1-weighted image was segmented using Unified Segmentation [114]. Segmentation-based normalization parameters were implemented into this coregistered structural and functional data to be able to transform slightly different individual brain images into common MNI (Montreal Neurological Institute) space. Following normalization, resting state data were resampled into 3 x 3 x 3 mm³ voxels. As a result of excessive head movement defined as a cumulative translation or rotation >3mm or 3°, MRI data of 7 VP/VLBW subjects and 10 FT subjects were abandoned from further analysis. To measure motion-induced artifacts, temporal SNR (tSNR), point-to-point head motion, along with frame-wise displacement were evaluated for each

subject [115-117]. No significant differences between groups in terms of mean point-to-point translation or rotation of any direction (p >0.1), tSNR (p>0.25), and frame-wise displacement (p>0.3) by using two-sample t-tests. Considering intensive discussion about global brain signal removal effects on resting state fMRI [118,119], I did preprocessing with and without global brain signal regression separately to test stability of the results. Here I did not apply additional 'scrubbing' approaches to eliminate outliers in fMRI volumes [117], because elimination of non-contiguous time points may alter the inherent temporal structure of the data, hindering conventional frequency-based analyses of rs-fMRI data, as advised by some experts [120,121]. Therefore the fast Fourier transformation-based ALFF, the primary outcome of this study is not appropriate for scrubbing.

3.6 Data processing: outcome variables and statistical analysis

3.6.1 ALFF

As the first step of the analysis, several spurious variances, i.e., six head movement parameters, white matter, global brain signal, along with cerebrospinal fluid (CSF) signal intensities were regressed out from preprocessed resting-state fMRI data. Afterward, the resultant images were smoothed with a Gaussian kernel with a full-width at half-maximum (FWHM) of 6 mm. Next, following linear-trend removal, each given voxel was first converted the frequency domain using Fast Fourier Transformation to acquire the power spectrum. Then the ALFF was calculated by the power spectrum

that was averaged square root across 0.01–0.1 Hz at every voxel. Eventually, for standardization purposes, the ALFF of each voxel was then divided by the global mean of ALFF values inside the whole brain mask [79]. To explore statistical differences between groups, voxel-wise ALFF maps of all the subjects were integrated into a general linear model via implemented in SPM12, with the element 'group', and the covariates (nuisance variables) including 'gender', 'scanner identity', and 'frame-wise displacement'. Two-sample t-tests were used to test statistical differences ($p < 0.05$, corrected for family-wise error (FWE) at cluster-level).

3.6.2 Voxel-based morphometry (VBM) and ALFF

Voxel-wise gray matter volumes were processed using voxel-based morphometry as implemented in VBM8 (http://dbm.neuro.uni-jena.de/vbm.html) to further investigate its relationship with ALFF. T1-weighted images were adjusted for bias-field inhomogeneity, registered using linear (12-parameter affine) and nonlinear transformations. Here, I only contemplated nonlinear changes so that next step normalization did not have to concern impact of different head sizes. Structural MRI images were segmented into gray matter (GM), white matter, and cerebrospinal fluid within the identical generative model. The consequent GM images were modulated to account for structural changes caused by the normalization procedure then resampled to a voxel size of 1 × 1 × 1 mm. Finally, resulting images were smoothed with a 6mm full width half maximum (FWHM) Gaussian kernel. For group comparisons, voxel-wise two-sample t-tests were performed ($p < 0.05$

FWE-corrected), controlling for gender and scanner identity.

Recent findings indicate that structural differences in gray matter volumes may affect functional activations derived from fMRI signals between group differences [122,123]. To guarantee the functional essence of latent ALFF changes in premature born adults, post hoc voxel-wise linear regression analysis was performed to explore the effect of GMV on alterations in ALFF, namely residualizing ALFF values. More specifically, resulting residuals correct for non-linear effect of brain structure changes on ALFF, were implemented in general linear models (GLM) voxel wisely. Confidence was prior specified at p<0.05, family-wise error (FWE) cluster-level corrected. Sex, scanner identity and FD were modeled as nuisance regressors.

3.6.3 The connection between ALFF with overlapping gray matter, prematurity scores, and cognitive performance variables.

To evaluate whether the connection between cerebral function and structure was distinct for overlapping aberrant ALFF and GMV, partial correlation analysis between group different ALFF clusters and underlying gray matter was conducted. First aberrant mean ALFF was saved as masks of regions of interest (ROIs), then they were extracted from all the 94 VP/VLBW subjects. Subsequently averaged GMV images were resampled to the same voxel size as averaged ALFF. Finally gender and scanner identity were regressed out to calculate the relationship between averaged ALFF and averaged GMV values. Furthermore, to analyze the relationship between abnormal ALFF and

prematurity scores as well as neurocognitive performance, exactly the same methodological of averaged ALFF values were extracted, and associated with birth-related variables (namely GA, BW, INTI and OPTN), and the adult neurocognitive performance variables (namely verbal IQ, performance IQ and full-scale IQ), respectively. These associations were assessed using partial correlation analyses generated by SPSS (IBM, Statistical Package for the Social Sciences 24). In every partial correlation approach, gender, scanner identity, and frame-wise displacement (FD) were controlled as covariates of no interest, and the significance threshold was set at 0.05.

3.7 MVPA

3.7.1 Multivariate Pattern Classification Analysis

3.7.1.1 Preprocessing of multivariate pattern classification analysis with MRI data

I used pattern recognition tool NeuroMiner (www.pronia.eu/neurominer) to build a entirely automated machine learning pipeline, in which I (1) construct sets of predictive neuro-functional features from ALFF and GMV data separately, and (2) learned decision rules based on these neuroimage features then build algorithm to separate VP/VLBW from FT at the single-subject level. The elaborate preprocessing steps were below: Firstly, I performed preprocessing steps with ALFF and GMV, including smoothing (setting 4mm, 6mm, 8mm and 10mm parameters), regression out age, gender and scanner effects. I also estimated total intracranial volume (TIV) in order to

correct for different head size and volume in GMV analysis. Then principal component analysis (PCA) [124] was used to retain 80% of the variance in each CV1 (a subordinated inner CV cycle in the nested CV design) training partition for feature dimensionality reduction and discard noisy information, at last scale voxel-wise to [0, 1]. These preprocessing optimization combinations were completely embedded cross validation framework [125].

3.7.1.1. Repeated double cross-validation (rdCV)

The performance of a classification model on new, unseen test cases is representatively estimated using k-fold cross-validation (CV), in which the study population is divided into k non-overlapping folds and each fold is hold out to repeatedly calculate once to estimate the classifier's performance on test data while the rest k-1 folds are utilized to train the classifier's decision rule. Since in many real-world applications the optimal parameters of this decision rule are unknown, CV is utilized to automatically retrieve those parameters that estimate the best model on the validation data. However, this strategy may violate the rule of dissociating the training from the test data and may therefore lead to overfitting of the predictor's generalization capacity to unseen cases [126]. Here I used repeated, double cross-validation (rdCV) strategy to guard against information leakage between training and test data, and generate models with a higher likelihood of successful generalization to unseen data [127]. In details, the aforementioned analyses steps were embedded in a 5x10-fold cross-validation at the outer cycles (CV2) and a 1x10-fold cross-validation at the inner cycles (CV1) of repeated, double CV.

Material and Methods

After 80% features selected by greedy forward search wrapper [128] in the CV1 training and testing data, they were fed to a linear L2 regularization, L1-Loss SVC configured in the LIBSVM toolbox (https://www.csie.ntu.edu.tw/~cjlin/libsvm/), then selecting the best performing variable ('winner takes it all') from the pool. I weighted hyper-plane in uneven group sizes in the meantime. The six slack/regularization C parameters (0.125, 0.25, 0.5,1, 2, 4) were predicted in the inner loop of the cross validation.

Then unseen CV1 and CV2 test subjects were processed by sequentially applying all parameters generated by training to the test set. The classifier decided a test subject's geometric structure reference to the learned decision boundary, leading to a group membership score and predicted categories. To be precise, this analysis sequence was iterated for every CV1 training subdivision in a given CV2 training fold, thus producing an ensemble classifier which calculated a CV2 test subject's group membership by averaging the decision scores of its base learners. Ultimately, a CV2 test set membership was predicted by an ensemble classifier that equalized the decision scores of those 500 CV1 base learners in the repeated nested CV, in which the subjects had not been employed in the training procedure.

The aforementioned described classification procedure was put independently into both ALFF and GMV for all the subjects, resulting in two types of decision scores, one working on the structural GMV and the other dependent on the resting state ALFF. The fusion of the data domains was conducted by taking the average of the two modalities of decision scores, generating in a multi-

modal class membership scores individually obtaining from the multimodal

class membership.

3.7.1.2 Computation of voxel-level probability maps

Voxel probability maps (VPM) were subsequently visualized for every contrast

reflecting the degree of consistency and reliability of the subgroup traits

according to previous research [127]. In more detail, to visualize the average

decision function, NeuroMiner implements the procedure described in

Koutsouleris et al. [127], involving: (i) In PCA space, the weight vector (w) of

each SVM model was projected back to voxel space. This calculation was

worked for each training folds in the inner cross-validation (CV_1) cycle,

generating in 10 voxel-level images for the specific training division on the

outer (CV_2) loop. (ii) The volumes composed of average and standard error

from 10 voxel-level w images were computed. (iii) For each CV_2 partition, the

average weight vector was binarized, which means voxels with an absolute

value greater than their corresponding standard error multiplied by 1.96 were

set to one, if not set to zero. Therefore this thresholding procedure was driven

by only those voxels that authentically contributed to the average brain

functional and neuroanatomical decision boundary of a given CV_2 partition at

the 95% confidence interval. (iv) The summation of resulting binary images

across all CV_2 partitions was divided by the number of partitions, hence

generating a single map defined by every voxel's probability of credibly

contributing to the average cerebral decision boundary across the whole

procedure. (v) Voxels probability >95% were projected onto the standardized

Material and Methods

MNI template using the MRIcron software package

(http://www.sph.sc.edu/comd/rorden/mricron/).

3.7.2 Support vector regression analysis

Regarding the clinical moderator analyses, a v support vector regression (v-SVR) was employed to forecast the SVM decision scores of single modality based on clinical variables across 92 VP/VLBW individuals (table 1; for more details). Likewise to the classification process an rdCV framework (10x10 in CV1, 10x10 in CV2) was applied to generate an unbiased prediction of the method's performance. After the features of each CV2 fold were scaled to a range of [0, 1], each case with a NaN value, is conducted with a multivariate statistical technique, e.g. k-Nearest Neighbor-(k-NN) imputation to fill the missing values in the data [129]. Subjects in the source subset were sorted according to their similarity with the target subject using the Euclidean distance to identify the 7 nearest-neighbor subjects that are close to the subject with the NaN value in the multivariate space. Then, the median of the given feature values in the 7 nearest neighbors was computed and filled the missing value with this median value. This process was repeated until all missing values were filled with the respectively computed nearest-neighbor medians. I always used the original, non-imputed training matrix for the imputation.

Then the training matrix after scale and imputation was put into a greedy forward search wrapper [128], which follows a simple, yet powerful hill-climbing logic to identify the most parsimonious subdivision of variables within the

variable pool, thus providing maximum prognostic performance with the smallest amount of predictive features. More specifically, the wrapper algorithm used a pre-specified classification model to evaluate the predictive value of each variable in the pool, then extracted the most predictive variable and reiterated over the remaining variable pool to select the 2nd best performing variable, which was added to the first one. This process was reiterated until the 80% optimal variable subspace had been identified, then the best performing variables ('winner takes it all') from the pool was selected. The selected preprocessing clinical features were used to prognosticate the group membership scores with a v-SVR as implemented in the LIBSVM along with parameters setting v = [0.2, 0.5, 0.7] and C= [0.015625, 0.0625, 0.25, 1] to estimate in the CV1 training framework.

3.7.3 Correlation between SVM decision scores and clinical variables

Furthermore, a univariate Spearman correlation analysis was carried out in the VP/VLBW group to explore whether demographic (maternal age, age and sex), prematurity (namely GA, BW, hospital days, OPTN, INTI, DNTI) and cognitive performance variables (namely full-scale, verbal, and performance IQ) correlated with decision scores of ALFF and GMV separately.

3.7.4 Performance evaluation

Evaluation measures of classification performance usually include sensitivity, specificity, accuracy, balanced accuracy (BAC) and Receiver Operating

Characteristic (ROC) curve. Sensitivity is calculated as the TP / (TP + FN) and

is defined as the proportion of actual positive cases correctly identified. Here

TP means the number of true positives and FN is the number of false

negatives. Specificity is computed by the TN / (TN + FP) and is referred to the

proportion of the negatives cases correctly classified. TN is defined as the

number of true negatives and FP represents the number of false positives.

Accuracy is one of the most gold standard to evaluate classification models

and reframed as the overall amount of correct classifications across the

groups. It is calculated in terms of (TP + TN) / (TP + TN + FN + FP). Balanced

accuracy (BAC) is known as the amount of (sensitivity + specificity) / 2. The

Receiver Operating Characteristic (ROC) curve is plotted in function of the

true positive rate (Sensitivity) on Y-axis against the false positive rate (1-

Specificity) on X-axis for different cut-off points. Each different point on the

ROC curve is generated by using a different cut-off point and represents a

pair of (Sensitivity, 1-Specificity) corresponding to a particular decision

threshold. The table for terminology and derivations of classification outcomes

is showed as below.

	Condition positive	Condition negative		
Predicted positive	True positive (TP)	False positive (FP) Type I error	Positive predictive value=TP/(TP+FP)	Accuracy= (TP + TN) / (TP + TN + FN + FP)
Predicted negative	False negative (FN) Type II error	True negative (TN)	Negative predictive value=TN/(FN+TN)	
	Sensitivity =TP/(TP+FN)	Specificity =TN/(FP+TN)		

Material and Methods

Evaluation of regression performance usually includes R-squared, and the

Root Mean Square Error (RMSE). They are composed of two crucial sums of

squares: Sum of Squares Total (SST) and Sum of Squares Error (SSE). SST

estimates how far the data is from the mean (SST=$\sum$(y - $\bar{y}$)^2), and SSE

calculates how far the data is from the model's predicted values (SSE=$\sum$(y-

$\hat{y}$)^2). R-squared is calculated by the difference between SST and SSE, then

dividing that difference by SST (R^2=(SST-SSE)/SST). Compared to the mean

model, R-squared is the fractional improvement to predict from the regression

model but may increase the random noise in the model accompanied with an

increasing number of predictors. Adjusted R-squared is defined as the

modified version of R-squared which adjusts the predictor numbers and

penalizes the model complexity to regulate overfitting, and is explained as the

proportion of total variance and summarizes the explanatory power of the

regression model. Mean absolute error (MAE) as well as mean squared error

(MSE), calculated as the mean of the absolute value of the errors

($\frac{1}{m}\sum_{i=1}^{m}\left|(y_i - \hat{y}_i)\right|$) and the mean of the squared errors ($\frac{1}{m}\sum_{i=1}^{m}(y_i - \hat{y}_i)^2$) separately, are

two of the most common metrics to measure accuracy of continuous variables.

The RMSE quantifies the error rate of a regression model, and penalizes

large errors. It is defined as the square root of the average of squared

differences between prediction and observation ($\sqrt{\frac{1}{m}\sum_{i=1}^{m}(y_i - \hat{y}_i)^2}$) which

measure the average magnitude of the error.

4. Results

4.1 Socialdemographical and Sample Characteristics

Table 2 demonstrated demographic traits and clinical background variables between two groups. VP/VLBW sample did not differ from FT group with regard to age (p=0.277), gender (p=0.786), SES at birth (p=0.253) or maternal age (p=0.956). By design of the experiment, VP/VLBW grownups exhibited much lower GA (p<0.001), and BW (p<0.001). Inferentially they suffered more prematurity by showing significantly higher neonatal medical complications (DNTI, INTI and OPTN) (p< 0.001) and stayed in hospitals for longer time (p<0.001). At the same time, VP/VLBW individuals suffered more cognition deficiency during adulthood by displaying lower WAIS-III Full-Scale IQ scores (p=0.001), as well as Verbal IQ (p=0.001) and Performance IQ (p< 0.001).

Table 2. Sample characteristics

	Full-term born group (n=92)			VP/VLBW born group (n=94)			Statistical comparison
	M	SD	Range	M	SD	Range	
Gender (male/female)	53/39			56/38			p=0.786
Age (years)	26.8	±0.7	26-29	26.7	±0.6	26-28	p=0.277
GA (weeks)	39.7	±1.1	37-42	30.5	±2.0	25-36	p<0.001
BW (g)	3413	±433	2450-4670	1319	±309	630-2070	p<0.001
Hospital (days)	6.8	±2.4	2-15	72.8	±26.0	24-170	p<0.001
SES[a]	29/41/22		1-3	27/42/25		1-3	p=0.253
Maternal age	29.4	±5.2	18-42	29.4	±4.7	17-41	p=0.956
DNTI	-	-	-	53.9	29.3	8-149	-
INTI	-	-	-	11.7	3.8	3-19.8	-
TIV	1578.4	160.2	1204.6-1982.9	1507.2	143.9	1236.2-1860.6	P=0.002
Maternal age	29.4	±5.2	18-42	29.4	±4.7	17-41	P=0.956
Full-scale IQ[b]	102.9	±11.9	77-130	94.5	±12.9	64-131	P<0.001

Results

Verbal IQ[b]	106.5	±14.3	77-143	90.4	±14.0	62-137	P=0.001
Performance IQ[b]	98.5	±10.4	69-125	89.7	±13.8	56-118	P<0.001

Abbreviations: VP, very preterm; VLBW, very low birth weight; GA, gestational age; BW, birth weight; OPTI (neonatal), optimality score of neonatal conditions, Hospital, duration of hospitalization; DNTI, duration of Neonatal Treatment Index; INTI, Intensity of Neonatal Treatment (Morbidity) Index (inti1+inti2); TIV, total intracranial volume; SES, socioeconomic status at birth; maternal age, maternal age at birth; IQ intelligence quotient.

Statistical comparisons: sex, SES with χ^2 statistics; age, GA, BW, Hospital, maternal age, IQ with two-sample t-tests.

[a]1=upper class, 2=middle class, 3=lower class

[b]Data are from 90 VP/VLBW and 89 full-term subjects separately.

4.2 ALFF reductions and its relation with underlying brain structure

Two-sample t-tests were performed to investigate the difference of ALFF maps between two groups by revealing decreased and increased ALFF values voxel-wisely. Relative to maturely born adults, significant decreased ALFF were found in the left lateral temporal cortices with an extended cluster to insular cortex. Prematurely born grownups also showed increased ALFF in the thalamus (p<0.05, FWE cluster-level corrected) (Figure 2, Table 3). Additionally, I found decreased ALFF in the lateral temporal cortices of prematurely born adults even if omitting global brain signal removal (Figure 3), demonstrating that this main finding is not confounded by the preprocessing strategy of global brain signal removal.

Table 3. Group difference of ALFF brain between VP/VLBW and FT.

Results

Brain region	Cluster size	T-values	MNI			p-value
			x	y	z	
Thalamus	66	4.29	-3	-12	-12	0.006
Temporal-insular cortex	224	-6.65	-36	9	-24	<0.001
		-5.36	-54	-3	-15	
		-4.45	-54	6	0	

Statistical analysis: two-sample t-test (p<0.05, familywise error corrected for cluster-level), regression of effects of gender, scanners, and frame-wise displacement.
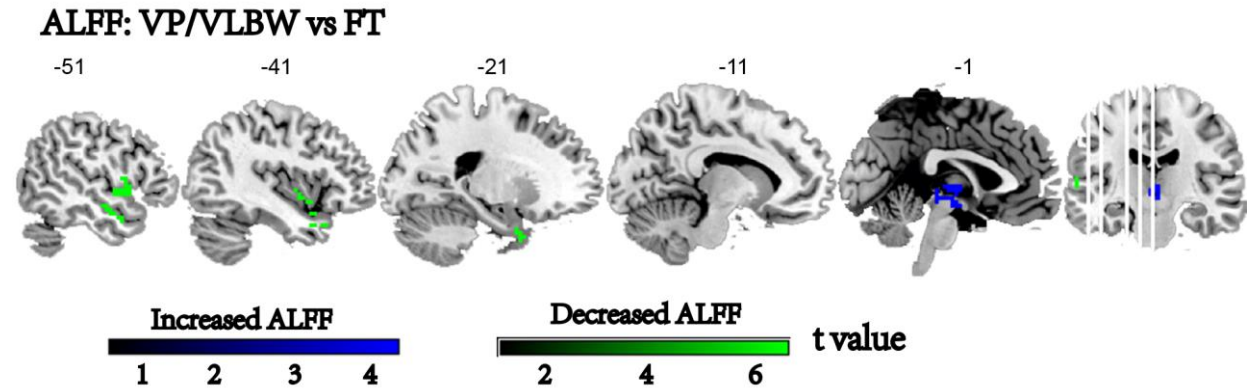

Figure 2. *ALFF topography of the prematurely born adults.*

Significance testing using two-sample t-test, p<0.05 (family-wise error corrected) based on statistical parametric map of group comparison for ALFF between VP/VLBW and FT born adults (Table 2). Color bars mean t-values which indicate the significant level of the ALFF in the VP/VLBW group. Abbreviations: ALFF, amplitude of low frequency fluctuations; FT, full-term; VP/VLBW, very preterm/very low birth weight.
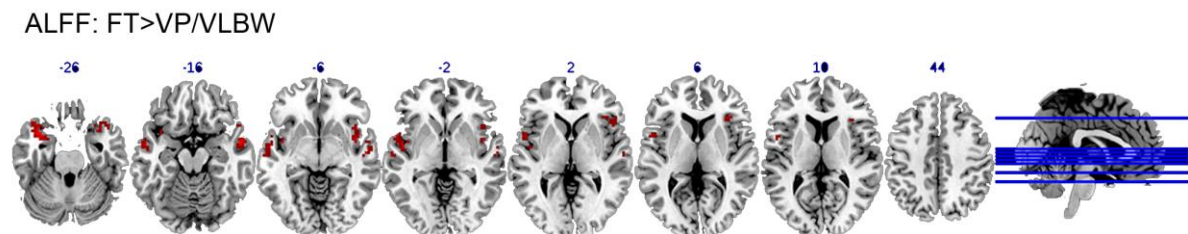
Figure 3. *Aberrant ALFF in the prematurely born adults without global signal correction.*

It still showed reduced amplitude of low frequency fluctuations (ALFF) in temporal cortices in prematurely born adults (two-sample t-test, p<0.05, FWE cluster-level correction).

To further explore the functional nature of ALFF reductions that are not fully attributed to underlying GM volume, I utilized VBM analyses of sMRI data to control for the confounding effects of volumetric changes in VP/VLBW born adults (Fig. 4). The comprehensive steps were described as below: First,

volume reductions were found in the VP/VLBW group mainly in temporal cortices and subcortical structures such as the thalamus and basal ganglia (Fig. 4A, Table 4). Spatial overlap of both modalities was in the left lateral temporal cortices and thalamus. The left lateral temporal cortices were characterized by ALFF and VBM reductions, and the thalamus had increased ALFF but decreased VBM (Fig. 4B). Second, after regression voxel-wisely VBM scores by two-sample t-test, residualized ALFF reductions still showed in the left temporal cortices but displayed as a fewer voxel-wise cluster in VP/VLBW, while increased ALFF in the thalamus did not retain (Fig. 4C). This result indicated that ALFF reductions in the left temporal cortices are not completely accounted for underlying volume loss but due to physiological nature.

To determine the relationship between temporal ALFF reductions with prematurity, partial correlation analyses were performed between averaged ALFF scores based on different group clusters and prematurity factors (i.e., GA, BW), along with medical complications at birth (INTI, OPTN) in the VP/VLBW sample. Figure 5 showed positive correlations between ALFF in the left temporal cortices and BW (r=0.289, p=0.007), but negative relationship between the left temporal cortices and INTI (r=-0.256, p=0.018), demonstrating that decreased ALFF in the temporal cortices were closely related with prematurity and medical complications.

To further assess the association between the temporal ALFF reductions and the overlapped fundamental brain structure, exactly the same methodological

Results

approach above was conducted between averaged ALFF values and VBM values in the VP/VLBW group. Partial correlations between ALFF and VBM values are displayed in Fig. 4D, which showed a positive relation between ALFF and VBM values in the left lateral temporal cortices (r=0.231, p=0.029), indicating that reduced ALFF was closely related with underneath decreased brain volume in temporal cortices. To investigate the relationship between rs-fMRI BOLD fluctuations and cerebral structure is particular for prematurely born adults in temporal cortices, extra partial correlation analysis for the connection between ALFF and VBM across full-term born group was performed. The result didn't show significant correlation in FT group, indicating the connection between rs-fMRI BOLD fluctuations and underneath cerebral structure in temporal cortices is unique to prematurity.
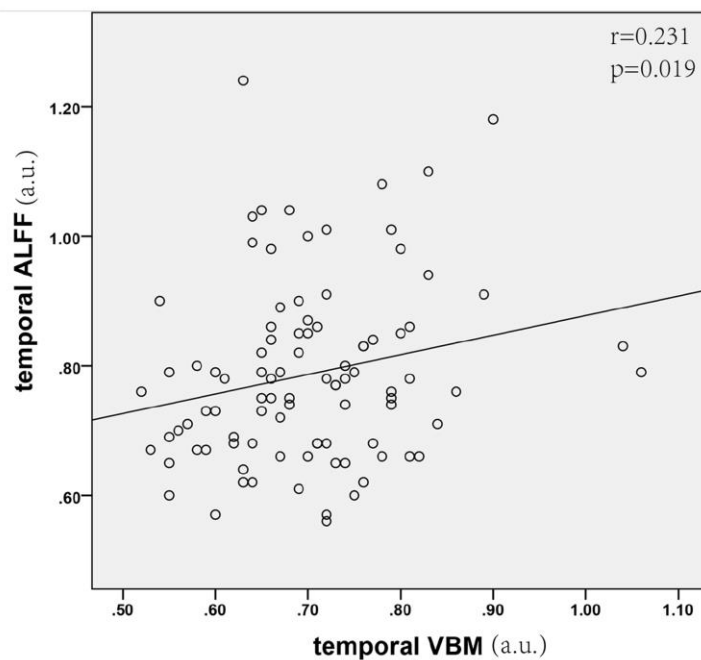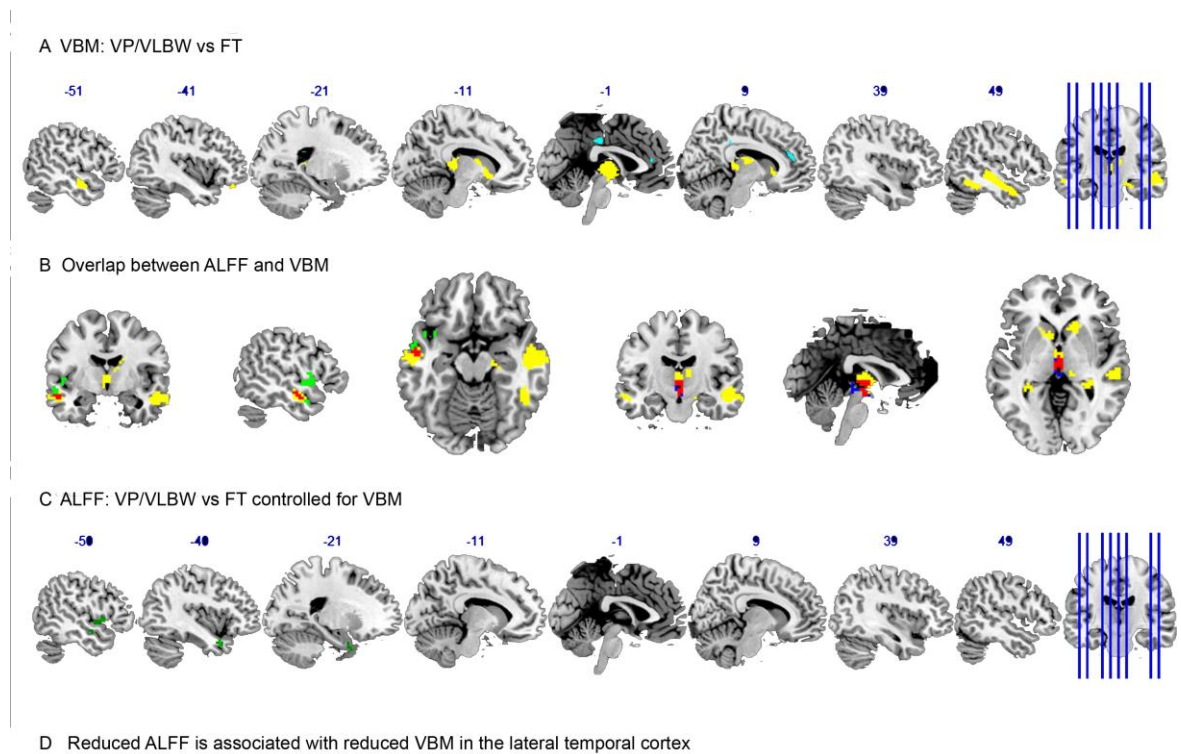
Results

A VBM: VP/VLBW vs FT

B Overlap between ALFF and VBM

C ALFF: VP/VLBW vs FT controlled for VBM

D Reduced ALFF is associated with reduced VBM in the lateral temporal cortex

r=0.231
p=0.019

Figure 4*. ALFF and VBM changes in prematurely born adults.*

A) Significance testing using two-sample t-test, p<0.05 (family-wise error corrected) based on statistical parametric map of group comparison for VBM between VP/VLBW and FT born adults (Table 4). Reduced VBM on VP/VLBW group in yellow, increased VBM in turquoise. B) Superimposed (red) of alterations in ALFF and VBM (only VBM reductions in yellow) in prematurely born adults. C) VBM-residualized ALFF reductions in prematurely born adults, corrected with FWE after two-sample t-test. D) Scatterplots showing the association between temporal cortices ALFF reductions (vertical axis) change along with temporal cortices VBM reductions (horizontal axis) by partial correlation, p<0.05. Abbreviations: ALFF, amplitude of

Results

low frequency fluctuations; FT, full-term; VBM, voxel-based morphometry; VP/VLBW, very preterm/very low birth weight.

Table 4. Aberrant brain gray matter volume in very preterm/very low birth weight (VP/VLBW) and full-term(FT) adults.

Brain region	BA	Cluster size	T values	MNI			p value
				X	Y	Z	
FT born > VP/VLBW born							
MTG(R)	21	3178	-10.72	57	-10	-18	<0.001
			-9.52	66	0	-21	
			-9.32	60	6	-26	
Thalamus(R)	-	3578	-9.18	17	-30	15	<0.001
			-7.55	9	-6	16	
			-6.89	33	-36	0	
Fusiform gyrus(R)	37	395	-7.05	50	-51	-14	<0.001
			-7.01	50	-40	-18	
Thalamus(L)	-	763	-8.62	-18	-36	13	<0.001
			-6.65	-33	-40	-3	
			-5.45	-27	-31	-9	
MTG(L)	21	690	-7.83	-62	3	-23	<0.001
			-7.39	-54	-6	-17	
			-5.52	-68	-9	-15	
PCC(L)	23	166	-7.53	-9	-46	15	<0.001
Frontal pole(L)	10	133	-7.15	-39	42	-23	<0.001
Hippocampus (R)	36	67	-5.54	18	-18	-14	0.004
			-4.95	26	-18	-18	
FT born < VP/VLBW born							
ACC	32	93	6.84	8	42	16	<0.001
			5.30	-5	41	15	
PCC(L)	30	1294	6.75	-32	-46	10	<0.001
			6.66	-17	-42	28	
			6.16	-14	-33	25	
aPFC(R)	10	46	7.53	35	45	-9	0.002
Fusiform gyrus(R)	37	83	5.69	35	-48	-17	0.010
vmPFC(L)	11	28	5.53	-8	50	-32	0.004
Temporal pole(L)	38	45	5.78	-33	24	-33	0.001

Abbreviation: ACC: anterior cingulate, PCC: precuneus, MTG: middle temporal gyrus, aPFC：anterior medial prefrontal cortex, vmPFC: ventral medial prefrontal cortex

Results

Statistical testing: two-sample t-test of voxel-based morphometry, controlled for gender and scanner identity, p< 0.05, FWE-corrected.
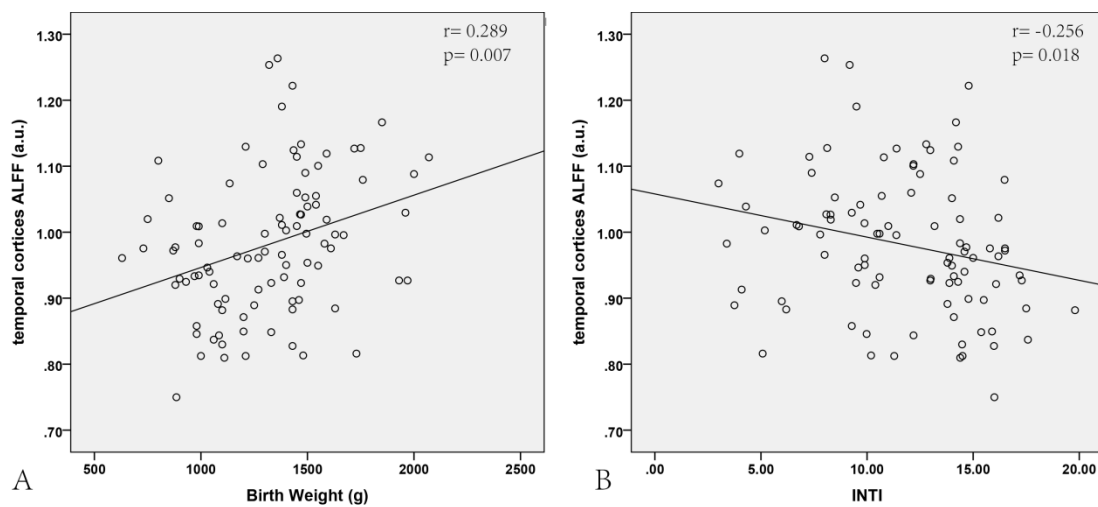

Figure 5. *The relationship between decreased ALFF in temporal cortices and birth-related variables in prematurely born adults.*

Decreased ALFF in temporal cortices (see Fig.2) is positively correlated with BW and negatively correlated with INTI, partial correlation, p<0.05. Abbreviation: BW, birth weight; INTI, Intensity of Neonatal Treatment (Morbidity) Index (inti1+inti2).

4.3 The relationship between ALFF reductions and adult neurocognitive performance

To test if correspondent brain changes in temporal ALFF reductions are related with adult neurocognitive performance, averaged ALFF values and adult neurocognitive performance via partial correlation analyses controlling for gender, scanner identity and FD in the VP/VLBW group only were conducted (Fig. 5). The result showed positive correlation between ALFF and performance IQ (r=0.275, p=0.011) and full-scale IQ (r=0.267, p=0.013), demonstrating the cognitive associative with ALFF reductions in temporal cortices after prematurely born.
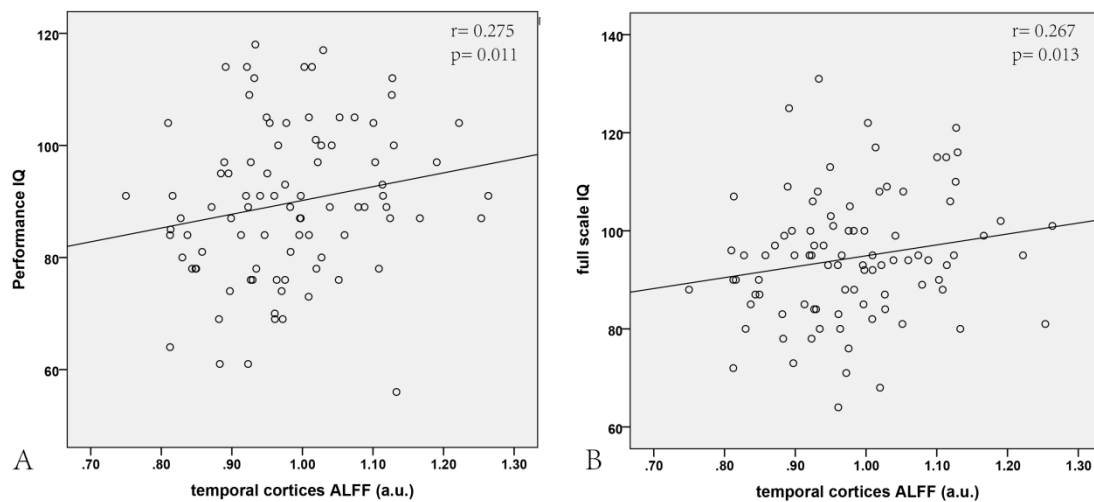
Results

Figure 6. *Temporal cortices ALFF and IQ in prematurely born adults.*

Reduced temporal cortices ALFF (see Fig.1) are associated with impaired performance IQ (A) and full-scale IQ (B), partial correlation, $p<0.05$. Abbreviation: IQ, intelligence quotient.

4.4 Patterns of aberrant GMV in the VP/VLBW adults

Multivariate pattern classification via SVM based on individual GMV maps separated VP/VLBW and FT participants with balanced accuracy of 80.72% (specificity 73.40%, sensitivity 88.04%, Area Under the Curve: 0.90) (Table 5). Distinguishing patterns of increased and decreased GMV, respectively, which visualize this group separation, indicate multi-variate patterns of interrelated volume decreases and increases in prematurely born adults (Figure 7). Patterns of decreased GMV in the VP/VLBW group compared with the FT group were in the bilateral inferior and middle temporal gyri, thalamus, caudate, and hippocampus. Patterns of increased VBM were in the superior temporal gyri, medial and lateral prefrontal cortices, precuneus/posterior cingulate cortices, and occipital regions.

Table 5. Classification performance of very preterm/very low birth weight (VP/VLBW) based on ALFF, GMV and bagging of two modalities.

Results

Binary classifiers	GMV	ALFF	bagging
TP	69	68	68
TN	81	76	80
FP	11	16	11
FN	25	26	25
Accuracy	80.7	77.4	80.4
Sensitivity,%	73.4	72.3	73.1
Specificity,%	88.0	82.6	87.9
BAC	80.7	77.5	80.5
AUC	0.90	0.85	0.91
PPV	86.3	82.0	86.1
NPV	76.4	74.5	76.2

Abbreviations: ALFF, amplitude of low-frequency fluctuations; GMV, gray matter volume; FN, false-negative; FP,false-positive; FPR, false-positive rate; AUC, area under the curve; BAC, Balanced Accuracy; NPV, negative predictive value; PPV, positive predictive value; TN, true-negative; TP, true-positive.
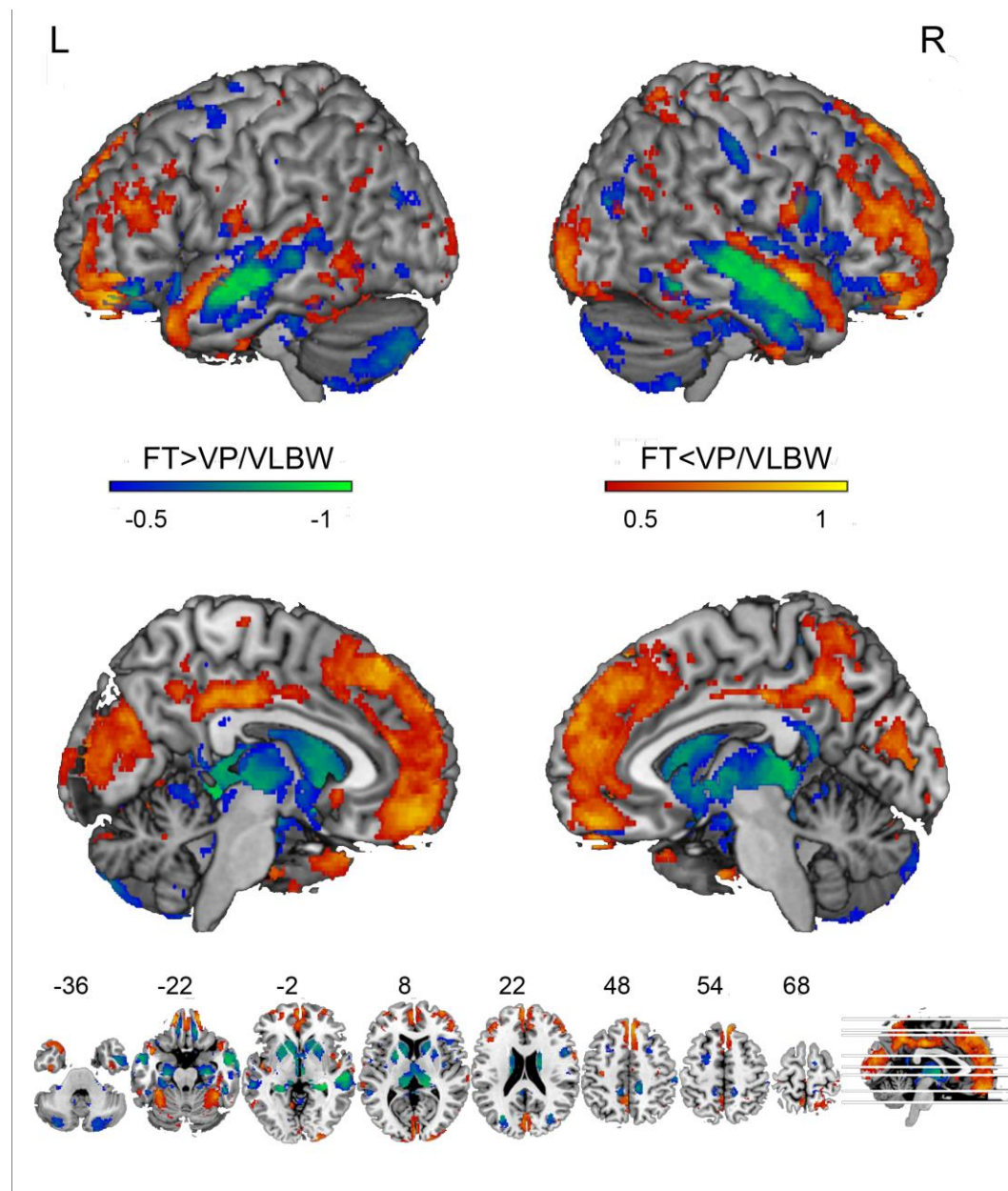
Results

Figure 7. *Voxel probability map (VPM) of 95% authentic contributions to the FT versus VP/VLBW decision boundary using GMV*.

Voxels with a probability of >50% were mapped onto the MNI template using the MRIcron software package (http://www.mccauslandcenter.sc.edu/mricro/mricron/).

4.5 Patterns of aberrant ALFF in the VP/VLBW adults

Multivariate pattern classification based on individual ALFF maps separated

VP/VLBW and FT participants with balanced accuracy of 77.47% (specificity

Results

72.34%, sensitivity 82.60%, Area Under the Curve: 0.85) (Table 5). Patterns

of decreased ALFF in the VP/VLBW group compared with the FT group were

in the temporal poles, superior temporal gyri, and inferior frontal gyri (Figure

8). Patterns of increased ALFF were in the thalamus and the superior parietal
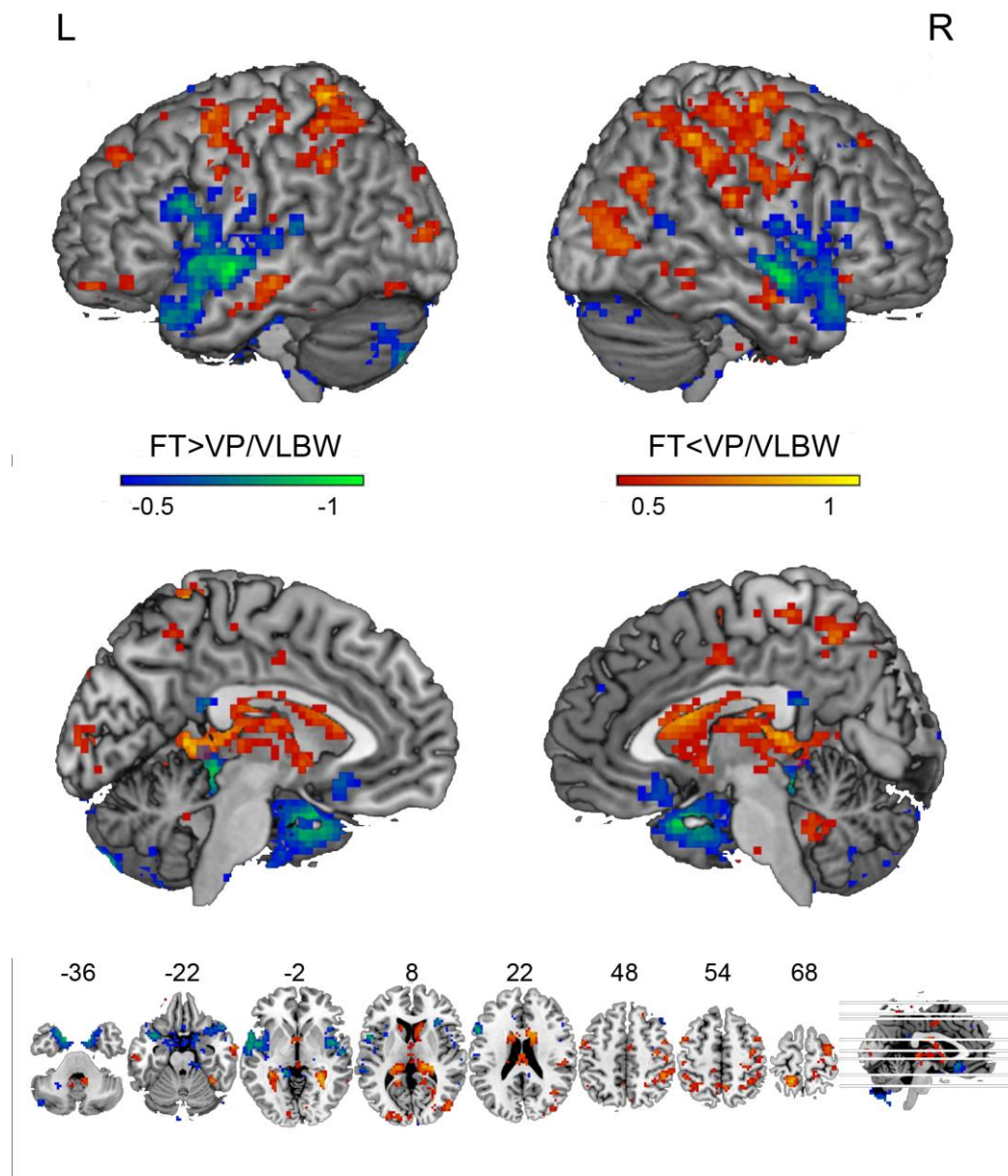
lobes extending to the premotor cortices (Figure 8).

Figure 8. *Voxel probability map (VPM) of 95% authentic contributions to the FT versus VP/VLBW decision boundary using ALFF.*

Results

Voxels with a probability of >50% were mapped onto the MNI template using the MRIcron software package (http://www.mccauslandcenter.sc.edu/mricro/mricron/).

4.6 Overlapped regions between patterns of aberrant brain volumes and ongoing activity by MVPA

Since quantitative relationship between mutual structural and functional differences have been conducted in the univariate analysis, it is necessary to further extend their correlation by MVPA. Therefore I calculated the superimposed voxel probability maps from both modalities on the basis of the following procedures: First, any significant clusters of voxel probability maps calculated after post-hoc analysis from both modalities were saved as images in SPM12, then these brain masks were binarized between two thresholds, -1~-0.5 for negative range or 0.5~1 for positive range. Second, superimposed the statistical maps obtained from both entities were resampled to the same dimension, subsequently multiplied with each other with ImCalc. In this way, only voxels indicating significant group differences in either domain remained. By this means, consequent overlap only involved voxels that displayed significant differences in both spontaneous cortical dynamics and underlying anatomical gray matter (Figure 9).
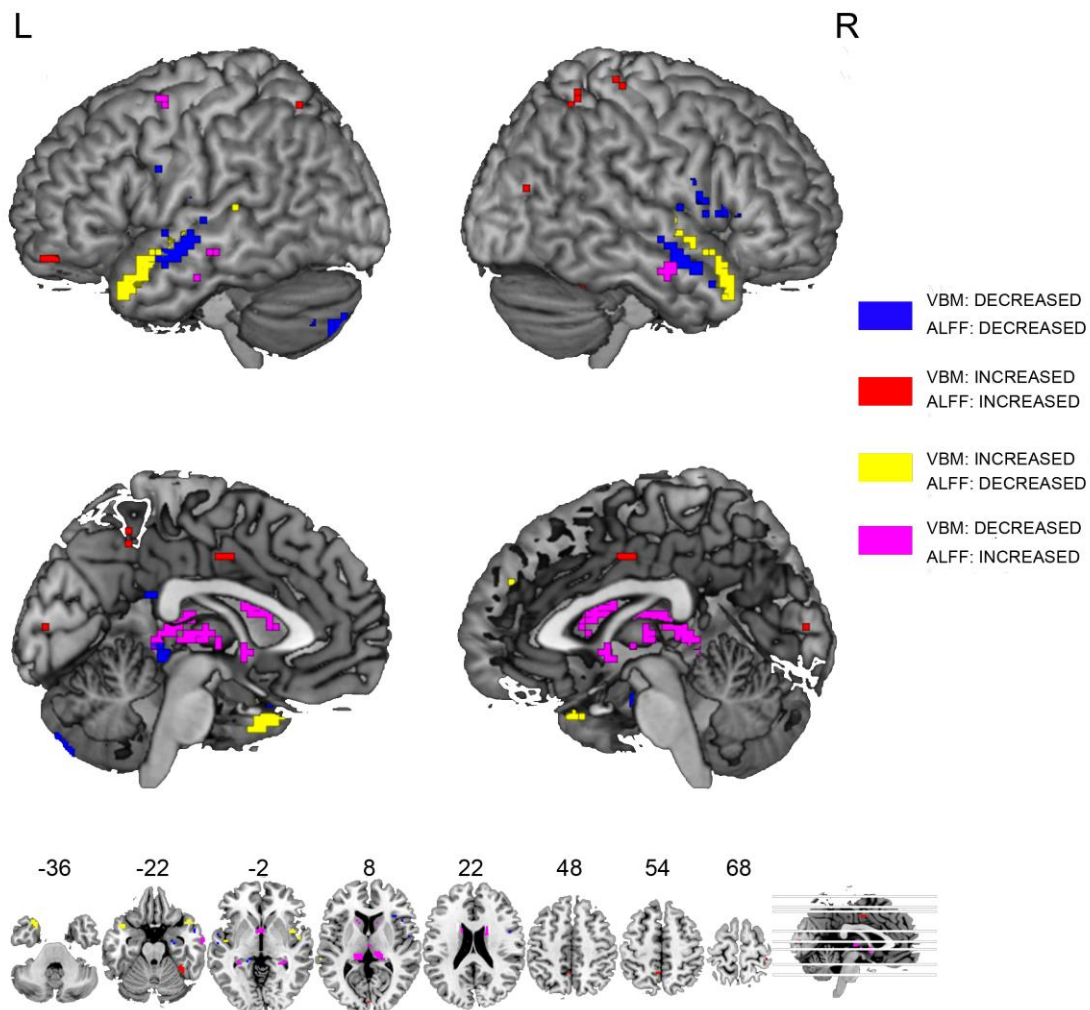
Results

Figure 9. *Voxel probability map of overlapped regions between amplitude of low-frequency fluctuations (ALFF) of resting-state fMRI and VBM, to the decision boundary of VP/VLBW (very preterm/very low birth weight born) versus FT (full-term born) group.*

Blue represents decreased VBM and ALFF in both middle temporal gyri and the right insula. Red represents increased VBM and ALFF in the right fusiform gyrus and parietal lobes. Yellow represents areas with increased VBM but decreased ALFF in both superior temporal gyri and temporal lobes. Violet represents areas with decreased VBM but increased ALFF in subcortices, including thalamus and caudate nucleus. Voxels with a probability of >50% were mapped onto the MNI template using the MRIcron software package (http://www.mccauslandcenter.sc.edu/mricro/mricron/).

4.7 Patterns of aberrant brain volumes and ongoing activity, respectively, relate with clinical performance scores of prematurely born adults

Results

To investigate the link between clinical-performance scores and patterns of aberrant GMV and ALFF maps, respectively, both support vector regression and Spearman correlation analyses were performed. Concerning multivariate support vector regression, clinical-performance scores predicted ALFF- and GMV-based classification decision scores, respectively (ALFF: R^2 = 13.96%, r=0.37, P <0.001, T = 3.86, mean average error = 0.43; GMV: R^2 = 30.04%, r=0.56, P <0.001, T = 6.42, mean average error = 0.60) (Table 6). Across both imaging modalities, increased number of hospital days and lower BW was associated with more VP/VLBW likeness (Figure 10). For ALFF specifically, a lower performance IQ was associated with more VP/VLBW likeness and for GMV was associated with a higher total intracranial volume.

Table 6. Multiple demographical and clinical variables predict support vector machine (SVM) decision scores of ALFF and GMV separately only based on very preterm/very low birth weight (VP/VLBW) by using v-support vector regression (SVR).

nu-SVR	GMV	ALFF
COD(R^2)	30.94	13.96
Pearson r	0.56	0.37
P(t) value	<0.001(6.42)	<0.001(3.86)
MAE	0.6	0.43
MSE	0.5	0.4

Multiple clinical-performance variables and support vector regression (nu-SVR) was used to predict the decision scores in 94 VP/VLBW subjects based on grey matter volume (GMV) and amplitude of low-frequency fluctuation (ALFF), respectively of Table 5 and Figures 7 & 8. Clinical-performance variables were: gender, GA, BW, OPTI (neonatal), Hospital, DNTI, INTI, SES, maternal age, adult age, intelligence quotient (including verbal, performance and full-scale IQ) for both ALFF and GMV. TIV is only included in GMV group.

Abbreviations: ALFF, amplitude of low-frequency fluctuations; BW, birth weight; COD, coefficient of determination; DNTI, duration of neonatal treatment index; GA, gestational age, GMV, gray matter volume; INTI, intensity of neonatal treatment index; IQ, intelligence quotient;

MAE, mean absolute error; MSE, mean squared error; OPTI, optimality score of birth; SES, socioeconomic score; TIV total intracranial volume.

Concerning Spearman correlation, on the one hand, VP/VLBW likeness based on ALFF was related with BW, GA, hospital days, IQ, as well as the duration and intensity of neonatal treatment/morbidity index (DNTI and INTI); on the other hand, VP/VLBW likeness based on GMV was linked with BW, GA and hospital days as well as DNTI and INTI.

4.8 Bagging

Decision-based late fusion pattern classification resulting from two MRI modalities is able to distinguish between VP/VLBW and FT participants with 80.43% accuracies (balanced accuracy 80.52%, specificity 73.12%, sensitivity 87.91%, Area Under the Curve: 0.91) (Table 5). The result of bagging is similar to GMV based classifier performance, but better than ALFF based classifier performance.

4.9 Effect of Clinical Measures on Neuroimaging Results

Demographic, clinical, and cognitive variables were used in further analyses to explore the clinical relevance of classification models produced using GMV and ALFF data. Specifically, the v-SVR model predicted ALFF decision scores (R^2 = 13.96%, r=0.37, P <0.001, T = 3.86, mean average error = 0.43) and

Results

GMV decision scores (R^2 = 30.04%, r=0.56, P <0.001, T = 6.42, mean

average error = 0.6) (Table 6). The weight profile of clinical features resulting

from the SVR method indicates that, for both GMV and ALFF, more hospital

days and lower birth weight were related to the membership into the

VP/VLBW versus FT groups. When primarily combined with total intracranial

volume (TIV), the predictors explained 30% of the variance in the membership

scores related to the prediction of preterm status using GMV. For ALFF, when

primarily combined with performance IQ, the predictors explained 13% of the

total variance (Fig.8). These results validate the multivariate predictors and

associated brain maps by demonstrating: a) expected relationships between

measures of preterm severity that are associated with brain damage [2]; b)

discriminant validity by showing that performance IQ is related to brain

functioning whereas total intracranial volume is related to brain volume. The

relationship between performance IQ and ALFF maps have not been

demonstrated before and are particularly interesting because they highlight

the importance of assessing brain functioning in addition to brain structure
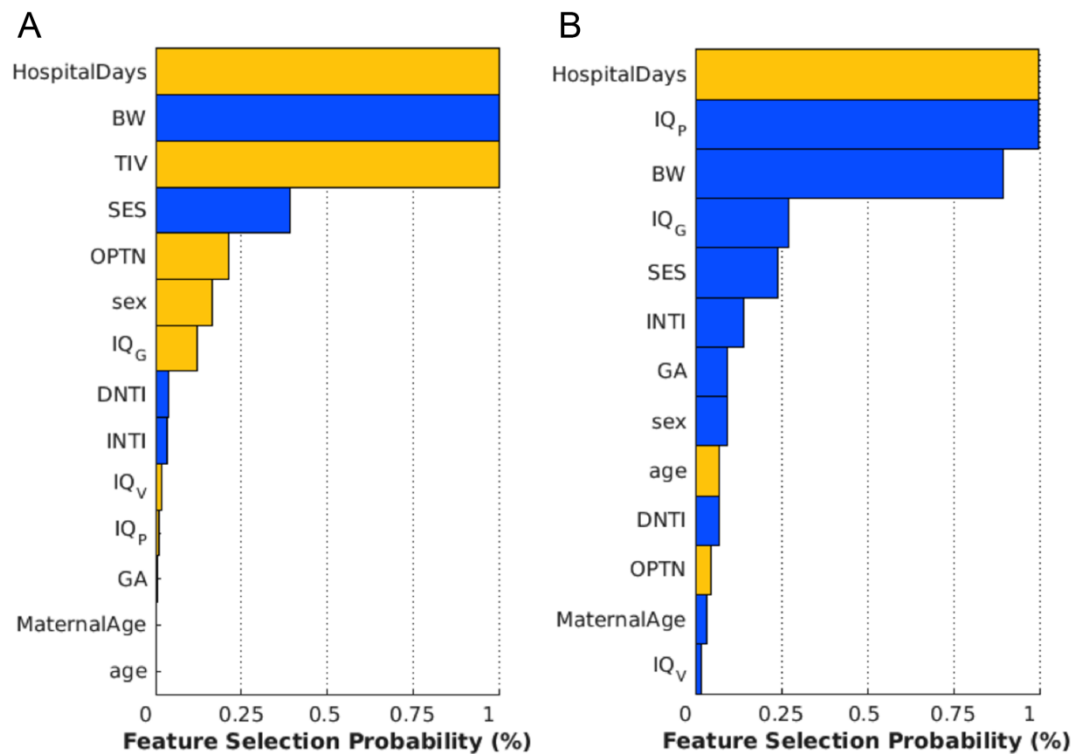
following preterm birth.

Results

Figure 10. *Feature selection probability displaying the most trustworthy clinical-performance contributions to the prediction of VP/VLBW decision scores from the GMV (A) and ALFF (B) brain analyses.*

Yellow bars indicate positive coefficients (i.e., higher values associated with higher VP/VLBW likeness) and blue bars indicate negative weights (i.e., lower values associated with higher VP/VLBW likeness). Features above a 50% selection threshold most reliably contribute to the models. Abbreviations: GA, gestation age; BW, birth weight; INTI, intensity of neonatal treatment index; DNTI, duration of neonatal treatment index; OPTN, optimality score of neonatal treatment; IQG, full scale intelligence quotient; IQp, performance intelligence quotient; IQv, verbal intelligence quotient; TIV, total intracranial volume.

I also tested whether SVM scores of two modalities were indeed related with prematurity and cognition, then I performed univariate Spearman correlation analysis of VP/VLBW group only between SVM decision scores and clinical variables. The result after Holm-Bonferroni correction showed that mean SVM scores of both modalities positively correlated with GA, BW, but negatively correlated with obstetric complications (i.e., days in hospital, DNTI). Besides, decision scores of ALFF were positively correlated with cognitive performance

variables (i.e., full-scale IQ and performance IQ). Decision scores of GMV

were negatively correlated with INTI (Table 7).

Table 7. Correlation between decision scores for VP/VLBW group based on GMV and ALFF, respectively, and clinical-performance scores.

Spearman correlation between decision scores for VP/VLBW group based on amplitude of low-frequency fluctuations (ALFF) and grey matter volume (GMV). The result of p-value was corrected by Holm-Bonferroni correction.

 * Correlation is significant at the 0.05 level. Abbreviations: IQ, intelligence quotient; ρ Spearman's rho; TIV total intracranial volume.

Clinical-performance Variables	GMV		ALFF	
	ρ	P	ρ	P
Maternal age	0.098	0.349	0.148	0.155
Gestational age	0.343	0.008*	0.283	0.030*
Birth weight	0.461	<0.001*	0.346	0.009*
Hospital days	-0.455	<0.001*	-0.354	0.005*
Intensity of Neonatal Treatment (Morbidity) Index	-0.289	0.035*	-0.195	0.236
Duration of Neonatal Treatment (Morbidity) Index	-0.408	<0.001*	-0.348	0.008*
Optimality score of neonatal conditions	-0.263	0.06	-0.171	0.3
Performance IQ	0.140	0.561	0.352	0.007*
Verbal IQ	0.158	0.685	0.161	0.26
Full scale IQ	0.145	0.684	0.303	0.024*
TIV	-0.115	0.542	--	--

5. Discussion

The aim of the research is to explore whether BOLD fluctuations and gray matter are varied during adulthood after premature birth by using univariate and multivariate pattern analysis. First, I explored the univariate model of the amplitude of low-frequency BOLD fluctuations (ALFF) and gray matter volume (GMV) making use of resting-state fMRI and structural data, from 94 VP/VLBW and 92 full-term born adults. The result showed decreased ALFF and GMV were superimposed in the left lateral temporal cortices, and positively correlated with each other only in VP/VLBW group. Furthermore, temporal ALFF reductions still retained after regress out decreased overlapping gray matter volume, indicating the functional nature of temporal ALFF decreases is not fully influenced by structural alterations. Second, to study patterns of inter-related brain changes after premature birth, I analyzed precisely the same data above by the use of multivariate pattern classification. The result showed distinct models of inter-related changes in both brain structure and ongoing activity after premature birth, which linked differently with individual infant birth- and adult performance-related factors. As far as I know, this is the first multimodal report composed of abnormal rs-fMRI BOLD fluctuations and gray matter volume in prematurely born individuals by combining univariate and multivariate analysis. In the following sections, I discuss these findings of univariate findings and MVPA results in more details separately.

Discussion

5.1 Univariate pattern analysis

ALFF, as the major outcome of this thesis, was observed decreased in the left insula as well as the lateral and anterior temporal cortices, apart from that increased thalamus was displayed in VP/VLBW sample (Figure 4, Table 4). Overlapping changes between ALFF and gray matter volume were present in the temporal cortices and thalamus (Figure 4A&B) of VP/VLBW adults. Particularly, decreased ALFF overlapped with decreased GMV in the lateral temporal cortices; at the same time, increased ALFF overlapped with reduced GMV in the thalamus. The structural brain abnormalities such as reductions in the thalamus and striatum as well as in temporal-insular cortices in VP/VLBW sample, is consistent with previous research [36,38,39,130]. Reduced ALFF in the left temporal cortices is not entirely dominated by underlying gray matter volume since ALFF still remained after controlling for varying structural alterations (Figure 4C). The above exhibition further supports the functional nature of ALFF reductions in temporal cortices in adults who are born prematurely. In clinical phenotypes investigation, temporal ALFF reductions associated with birth weight and INTI (Figure 5), independent of gender, scanners identity and framewise displacement effects, indicating that ALLF reductions are authentically related with prematurity and neonatal medical complications. At last, ALFF reductions in the temporal cortices correlated with neurocognitive impairment (including performance IQ and full-scale IQ) in prematurely born adults (Figure 6), illustrating the low frequent spontaneously fluctuations in temporal cortices vary with adulthood cognitive performance. Taking the above results into account, this thesis supports the view that amplitude of spontaneous BOLD signal coupling with brain structural changes

in the lateral temporal cortices is influenced by prematurity in the long term.

Preceding instances confirmed that ALFF, especially in the lateral temporal cortices, has a strong association with the effects of typical brain development as well as neuro-developmental disorders [76,131,132]. For instance, ALFF is sensitive to aging effects mainly in cortical midline structures, e.g. the anterior and posterior cingulate as well as in the lateral temporal cortices [76]. Itahashi, et al. found that autistic patients exhibited lower regional functional connectivity in lateral and inferior temporal cortices [132]. These temporal differences were more pronounced in schizophrenic patients, for example, increased ALFF in the left medial temporal region is assumed to reflect preexisting vulnerability to schizophrenia [133], while decreased ALFF in temporal cortices/ insula is discovered in the specific low frequency range [131] or connected with auditory hallucinations [134] in schizophrenic patients. In general, these accumulated evidences imply that ALFF variation, particularly in the temporal cortices, has been hypothesized strongly coincide with cerebral development. Therefore, it may be interpreted as a potential biological marker for neurodevelopmental brain disease. This sharing region in temporal ALFF cortices across distinct developmental conditions does not mean to identify common pathogenic mechanisms, but may account for converging on macroscopically similar amplitude of BOLD signal patterns in different brain stages.

GM alterations affected by prematurity, especially the temporal gyrus, are in line with previous studies that positive correlations were observed in GM of temporal cerebral regions and gestational age at birth [64,135-137]. My study

further supports that the thalamocortical system might play an essential role in the neurodevelopment and prematurity [34,138-140], by demonstrating long-lasting structural brain alterations of reduced temporal and subcortical gray matter volumes. These changes have been frequently described in preterm birth or low birth weight subjects [37,64,135,141-145]. Cortical development lies crucially on subplate neurons and their development [2,19]. Subplate neurons growth, in turn, has its highest rates in upper temporo-parietal regions including superior temporal cortices [146]. In this study, the degree of reduced thalamus-temporal GM changes was still observed in preterm-born adults, confirming long-term effects of prematurity on subplate neuron development.

Considering the closed relationship between BOLD signals and electrophysiological signals, decreased temporal ALFF may imply that correspondent fluctuations in slow neuronal activity on account of a portion of abnormal electrophysiological activity and have already been existed since prematurely born infants [147]. To acquire further supportive evidence to address the issue, more experiments of simultaneous EEG-fMRI focusing on premature born individuals are essential [148]. In addition, low frequency oscillations in ongoing neural activity and excitability are suggested to be a symbol of the fundamental neuronal activity of cortical networks [46]. For example, neocortical in-vitro slices result in spontaneous slow wave activity [149], and digital reconstructed cell assembly architectures simulate physiological BOLD signals [150]. These above findings suggest that synchronous BOLD oscillations are affected by basic single neurons and synaptic reverberation of the spiking activity, which in turn, varied long with structural changes [16,21,130]. Several studies based on premature human and

animal subjects further proved the hypothesis. For example, Ball and colleagues showed impaired thalamocortical connectome in preterm born infants via diffusion tensor imaging [130]. Further, Dean and colleagues demonstrated that abnormal cortical signals with diffusion imaging method were linked with impaired expansion of the dendritic arbor and reduced synaptic density in premature born sheep [16]. McClendon and colleagues showed that intimate relationship between hypoxia-ischemia/hypoxia in premature born sheep and dysmaturation of subplate neurons [21]. These accumulating studies imply that aberrant spontaneous cortical dynamics, e.g. temporal ALFF in prematurely born people might be associated with aberrant underlying gray matter structure in specific brain regions (Figure 4D). In turn, it is inferred that damaged cortical development after premature birth has an influence on fundamental spontaneous neuronal activity. In conclusion, premature birth might change slow oscillation in neural activity and excitability of temporal cortices via changes in underlying cortical microstructure. Further research needs to be tested through cortical micro-structural indices with ALFF-based measures.

Above all these points offer an overall debate for the connective between ALFF and slowly synchronized fluctuations in local synaptic activity. At the same time, ALFF might be partially affected by underlying cortical microcircuits. However, it is uncertain why ALFF alterations appear mainly in the temporal cortices. Other modalities focus on specific lateral temporal cortical alterations after premature birth have been described in published research, such as task-fMRI [59,151,152], resting-state fMRI [53,58], and diffusion

tensor imaging (DTI) [153,154] studies. Such coherent aggregation of alterations across different modalities after premature delivery affirms the idea that a fundamental firing of the local network showed on temporal cortices might be affected by prematurity and brain development.

Subplate neurons and their development are critically important for the earliest formed neurons and cortical formation [2,19-21]. As a transient cortical structure, such as the subplate zone below cortical layer 6, consists of distinct populations of subplate neurons and establishes intracortical and extracortical circuitries [20]. Heterogeneous populations of neurons in subplate zone work as the first cortical neurons, which include receiving ingrowing thalamocortical afferents [155], establishing pioneering cortical efferent projections [156], and projecting into the developing cortical plate [157]. Subplate neurons are critical for local microcircuit development and show the most active growth in gestational weeks 15-35. In particular, subplate neurons growth has the highest rates in lateral temporo-parietal regions [146]. As premature birth is acquainted to impact subplate neurons which are vulnerable to injury during prenatal stages [2,17-19], it is inferred that ALFF alterations in the temporal cortices might be explained as succeeding consequences of impaired subplate neuron in prematurity by showing overlaps between ALFF and gray matter reductions in lateral temporal cortices. To address this uncertain issue, future translational studies focusing on neurophysiology and neuropathology with animal models are necessary.

Discussion

5.2 Multivariate pattern analysis

In this investigation I extended the findings of cross-sectional studies on ALFF and GMV by support vector classification, and found that preterm birth could be predicted with a balanced accuracy of 80.7% using volumetric grey matter data, 77.4% using ALFF images and 80.5% using bagging, combining two different kinds of features (Table 5). Predictions using GMV were mediated by a pattern of subcortical and middle temporal reductions and volumetric increases of the lateral prefrontal, medial prefrontal, and superior temporal gyrus (Fig 5). Predictions using ALFF were associated with a pattern including increases in the thalamus, pre- and post-central gyrus, and parietal lobes, in addition to decreases in the superior temporal gyrus bilaterally (Fig 6). The reduced cortical (e.g. temporal-insular cortices) and subcortical (e.g. thalamus and striatum) brain pattern are consistent with previous univariate findings [75]. Furthermore, decreased ALFF in temporal lobes is also in line with previous univariate findings [75]. Compared with univariate findings, MVPA approach is better at detecting volumetric or functional inter-dependencies and more sensitive than individual-voxel-based methods by showing more brain regions affected in both modalities. Decision scores from each classification were predicted by the number of hospitalization days and neonatal birth weight (Fig 7), while specific relationships were found between GMV classification and total intracranial volume as well as between ALFF and performance IQ. When combined these influential elements, the clinical variables explained 31% of variance associated with the volumetric classification and 14% variance account for the ALFF classification (Table 8).

Discussion

Individuals born preterm could be differentiated from full-term individuals at an accuracy of 80%, highlighting extensive gray matter differences between the groups. The spatial brain patterns broadly agreed with previous univariate literature [36,38,139,158], but extended this research with a multivariate framework to demonstrate clearly differentiable networks of decreased and increased GMV. Decreased GMV was found in a pattern that centered on subcortical structures (thalamus, caudate, and hippocampus) and included the middle temporal gyrus. Increased GMV was detected in cortical structures that prominently involved the medial prefrontal cortices, dorsolateral prefrontal cortices, superior temporal gyrus, precuneus/posterior cingulate cortices, and occipital regions.

The differentiation between subcortical-temporal decreases and cortical increases could be interpreted as an interaction between primary brain disease and secondary neurodevelopmental disruption [2]. Some studies demonstrate neuronal loss and gliosis of the thalamus and basal ganglia [21,47,159], which is evident in reduced volumes on MRI in infancy [47,160]. Reduced volumes or disrupted connections of thalamo-cortex are also evident in childhood [161-164], adolescence and adulthood [38,165], indicating sustained damage and disruption of maturational processes [68,166]. While some other MRI studies reported localized increases or decreases in cortical volume in preterm children [144] and adults [64,167]. These mixed results can be attributed to secondary cascades of neurodevelopmental disruption across developmental windows resulting from damage to premyelinating oligodendrocytes, axons, thalamus, subplate neurons, and migrating GABAergic cells [2]. Other deep

Discussion

nucleus such as nucleus accumbens, due to dopamine synthesis capacity, was found to be negatively correlated with cognitive symptoms, which is identified by the Comprehensive Assessment of At Risk Mental States CAARMS [77]. Age effect on structural brain development might be another important effect. One of the first developmental MRI studies demonstrated that changes in GMV during development are not linear [168]: GMV generally increases as individuals pass from childhood into adolescence, and then subsequently decreases [169]. Two twin studies extended these observations, and attributed them to genes and environmental interactions [170,171]. Other research further demonstrated that the peak of GMV is reached in different lobes at different ages, primary motor and sensory cortices maturing first, complex laminar organization such as temporal and prefrontal cortices were later-maturing, possibly reflecting synaptogenesis and subsequent pruning [169,172]. This study demonstrated a clear pattern of extensive cortical volume changes in VP/VLBW participants compared to full-term subjects in early adulthood, suggesting that secondary neurodevelopmental disruption extends to synaptic pruning of mostly tertiary, heteromodal association cortex that is known to develop until 30 years of age [173].

Low-frequency BOLD fluctuations, as measured with ALFF, putatively arise from the spontaneous neural activity of microcircuits [46]. These fluctuations are sensitive to changes in brain development [52,174], aging [76], cognitive deficit [175,176], psychiatric illness [177-180], and neurodevelopmental disorders [132,181-183]. In this study, adults born pre- or full-term could be classified on the basis of these spontaneous fluctuations at an accuracy of 77.5% with a pattern

consisting of prominently decreased ALFF in the superior temporal cortices and temporal poles, along with increased fluctuation amplitude in thalamic, and pre- and post-central gyrus.

In previous univariate research in newborn infants, reduced ALFF compared to term infants was reported in a pattern consisting of the superior temporal gyrus bilaterally and motor areas, while increased ALFF has been reported in the precuneus and inferior temporal gyrus [174]. The results of the current study in grownups support this research by demonstrating persistence of reduced ALFF in bilateral superior temporal gyri. The findings also cohere with task-based and resting-state functional imaging research by showing specific functional deficits associated with temporal gyrus [53,58,59,151,152]. Combined, the results suggest that superior temporal functional deficits that are present in infancy persisted into early adulthood and inferred as a stable pathophysiological marker of preterm birth.

Increases in thalamic ALFF was also found in MVPA, which is consistent with previous univariate results in this thesis. Some evidence demonstrates that early thalamic damage is treated as a primary consequence of preterm birth [2]. Studies investigating altered functional thalamocortical connectivity have been conducted in preterm infants [49,140,184], children [185] and attributed alteration to be functional compensations for inefficient thalamocortical processing [184]. As such, the current finding suggests that primary thalamic damage may lead to increased spontaneously slow fluctuations in thalamus. This conclusion coheres with previous network-based approaches using the largely same

patient cohort [58], which also demonstrated increased thalamic functional connectivity by independent component analysis (ICA). Combined, the results suggest that increased ALFF is linked to increased functional connectivity in thalamus that persists into adulthood. Further research in preterm subjects from varied age groups is needed to test this hypothesis.

In addition to the increased ALFF in the thalamus, more widespread increases were found in the pre- and post-central gyrus. Similar primary damage and secondary disease effects may explain these results. Preterm subjects are particularly vulnerable to brain impairment resulting in the deep grey matter structures significantly reduced, e.g. basal ganglia and thalamus, and this brain pattern is observed across infants [139,160], children [144], adolescents [186] and adults [64]. Thalamocortical axons and white matter fibers are also disrupted by prematurity [34], undermining the widespread microstructural tissue and cortical connection of the preterm brain [187]. In particular, cortico-striatal-thalamic pathways connect sensorimotor areas [188-190], the suspected structural damage to the subcortical areas as found in this study could result in disrupted connectivity and subsequently increased amplitude of low frequency fluctuations. This hypothesis is supported by diffusion tensor findings indicating disruption to basal ganglia and to motor connections [191].

The temporal lobes were particularly crucial to the classification of adults born preterm in both the volume and ALFF data. Increased brain volume in the superior temporal gyrus was found in adults born preterm related to decreased ALFF, whereas reduced brain volume in adults born preterm was

Discussion

found for the middle temporal gyrus to be related to increased ALFF. In combination with the thalamic findings, these results highlight a consistent relationship in adults born preterm where decreased volume is associated with increased ALFF. A possible pathology that connects subcortical and temporal structures is associated with subplate neurons and their development [2,19-21]. Specifically, there is high growth of subplate neurons in the lateral temporal regions during development [146] and premature birth disrupts this [2,17-19], which could lead to primary damage (e.g., indicated by the middle temporal gyrus volume decrease) and secondary neurodevelopmental pathology (e.g., of the superior temporal gyrus).

Demographic, clinical, and cognitive variables were used in further analyses to explore the clinical relevance of classification models produced using volumetric and ALFF data. For both GMV and ALFF, more hospital days and lower birth weight were related to the membership into the preterm versus full term groups. When primarily combined with total intracranial volume, the predictors explained 30% of the variance in the membership scores related to the prediction of preterm status using GMV. For ALFF, when primarily combined with performance IQ, the predictors explained 13% of the total variance. These results validate the multivariate predictors and associated brain maps by demonstrating: a) expected relationships between measures of preterm severity that are associated with brain damage [2]; b) discriminant validity by showing that performance IQ is related to brain functioning whereas total intracranial volume is related to brain volume. The relationship between performance IQ and ALFF maps have not been demonstrated before

and are particularly interesting because they highlight the importance of

assessing brain functioning in addition to brain structure following preterm

birth.

6. Strength and Limitations

Several points are noteworthy when interpreting the results of this thesis. First, the BLS sample included is focus on VP/VLBW adults having lower grade newborn complications, fewer functional impairments, and better neurocognitive performance. People with more severe infant complications or intense lasting impairments in the initial BLS sample were more inclined to be eliminated in first MRI scanning or discontinued further interviews in the study. Therefore, cerebral changes relative with ALFF and GMV displayed here are conservative estimates of truly premature degrees. Second, the recruitment sample was restricted by MRI contraindications, e.g. pregnancy, severely impaired vision, as well as non-removable ferromagnetic implants (e.g. pacemakers). A record of acute neurological problems, for example, traumatic brain injury, cerebral inflammation, epilepsy, cerebral ischemia or hemorrhage, as well as chronic neurological disorders e.g. brain tumor and multiple sclerosis, were treated as interference factors excluded by this study design. Third, the present sample size consisted of 94 VP/VLBW and 92 FT adults is large enough to enhance the stability, credibility and generalizability to explain the result. Fourth, brain connectivity measures derived from rs-fMRI data might be affected by sample head motion during scanning and effects from four scanners, two sites in this study. The current research might be influenced by these potential confounds, which are controlled as strictly as possible.

Here I also combined a new technique, MVPA, which is a robust approach to

Strength and Limitations

accommodate and analyze massive, multi-dimensional neuroimaging datasets.

It is also proposed to generate data-driven decision boundaries to maximally

separate individuals of interest and identify intrinsic features within these data.

7. Conclusions

Consistent changes in thalamus-temporal cortex were discovered in both univariate and multivariate pattern analysis, further proved the vital role of subplate neurons in preterm brain development. In both methods, slowly fluctuating BOLD signal is reduced in lateral temporal cortices after very premature birth coupling with underlying microstructural changes. Using multivariate machine learning techniques, this study also suggests that volumetric imaging related to subcortical brain damage present in infancy also appears in early adulthood. What's more, MVPA ALFF patterns contain more information that quantifies spontaneous cortical dynamics with multi-voxel functional connectivity pattern discriminability, than univariate analysis across time series. These abnormalities are interconnected with cortical brain models that indicate secondary neurodevelopmental disruption is persisting into adulthood. SVM decision scores derived from neuroimage data related to preterm birth severity and intelligence variable validated the results.

Reference

1   Blencowe, H. *et al.* National, regional, and worldwide estimates of preterm birth rates in the year 2010 with time trends since 1990 for selected countries: a systematic analysis and implications. *The Lancet* **379**, 2162-2172, doi:10.1016/s0140-6736(12)60820-4 (2012).

2   Volpe, J. J. Brain injury in premature infants: a complex amalgam of destructive and developmental disturbances. *The Lancet Neurology* **8**, 110-124, doi:10.1016/s1474-4422(08)70294-1 (2009).

3   Volpe, J. J. Cerebellum of the premature infant: rapidly developing, vulnerable, clinically important. *Journal of child neurology* **24**, 1085-1104, doi:10.1177/0883073809338067 (2009).

4   D'Onofrio, B. M. *et al.* Preterm birth and mortality and morbidity: a population-based quasi-experimental study. *JAMA psychiatry* **70**, 1231-1240, doi:10.1001/jamapsychiatry.2013.2107 (2013).

5   Nosarti, C. *et al.* Preterm birth and psychiatric disorders in young adult life. *Archives of general psychiatry* **69**, E1-8, doi:10.1001/archgenpsychiatry.2011.1374 (2012).

6   Wardlaw, T. M. *Low Birthweight: Country, regional and global estimates*. (UNICEF, 2004).

7   Saigal, S. & Doyle, L. W. An overview of mortality and sequelae of preterm birth from infancy to adulthood. *The Lancet* **371**, 261-269, doi:10.1016/s0140-6736(08)60136-1 (2008).

8   Goldenberg, R. L., Culhane, J. F., Iams, J. D. & Romero, R. Epidemiology and causes of preterm birth. *The Lancet* **371**, 75-84, doi:10.1016/s0140-6736(08)60074-4 (2008).

9   Romero, R. *et al.* The preterm parturition syndrome. *BJOG : an international journal of obstetrics and gynaecology* **113 Suppl 3**, 17-42, doi:10.1111/j.1471-0528.2006.01120.x (2006).

10   Penn, A. A., Gressens, P., Fleiss, B., Back, S. A. & Gallo, V. Controversies in preterm brain injury. *Neurobiology of disease* **92**, 90-101, doi:10.1016/j.nbd.2015.10.012 (2016).

11   Jobe, A. H. & Bancalari, E. Bronchopulmonary dysplasia. *Am J Respir Crit Care Med* **163**, 1723-1729, doi:10.1164/ajrccm.163.7.2011060 (2001).

12   Rees, S. & Inder, T. Fetal and neonatal origins of altered brain development. *Early human development* **81**, 753-761, doi:10.1016/j.earlhumdev.2005.07.004 (2005).

13   Wolke, D. Psychological development of prematurely born children. *Archives of Disease in Childhood* **78**, 567-570 (1998).

14   Back, S. A. *et al.* Selective Vulnerability of Late Oligodendrocyte Progenitors to Hypoxia–Ischemia. *The Journal of Neuroscience* **22**, 455 (2002).

15   Buser, J. R. *et al.* Arrested preoligodendrocyte maturation contributes to myelination failure in premature infants. *Annals of neurology* **71**, 93-109, doi:10.1002/ana.22627 (2012).

16   Dean, J. M. *et al.* Prenatal cerebral ischemia disrupts MRI-defined cortical microstructure through disturbances in neuronal arborization. *Science translational medicine* **5**, 168ra167, doi:10.1126/scitranslmed.3004669 (2013).

17   Deng, W. Neurobiology of injury to the developing brain. *Nature reviews. Neurology* **6**, 328-336, doi:10.1038/nrneurol.2010.53 (2010).

Reference

18   Kinney, H. C. *et al.* Neuron deficit in the white matter and subplate in periventricular leukomalacia. *Annals of neurology* **71**, 397-406, doi:10.1002/ana.22612 (2012).

19   Salmaso, N., Jablonska, B., Scafidi, J., Vaccarino, F. M. & Gallo, V. Neurobiology of premature brain injury. *Nature neuroscience* **17**, 341-346, doi:10.1038/nn.3604 (2014).

20   Hoerder-Suabedissen, A. & Molnar, Z. Development, evolution and pathology of neocortical subplate neurons. *Nature reviews. Neuroscience* **16**, 133-146, doi:10.1038/nrn3915 (2015).

21   McClendon, E. *et al.* Transient Hypoxemia Chronically Disrupts Maturation of Preterm Fetal Ovine Subplate Neuron Arborization and Activity. *The Journal of neuroscience : the official journal of the Society for Neuroscience* **37**, 11912-11929, doi:10.1523/JNEUROSCI.2396-17.2017 (2017).

22   Nagy, Z. *et al.* Preterm children have disturbances of white matter at 11 years of age as shown by diffusion tensor imaging. *Pediatric research* **54**, 672-679, doi:10.1203/01.PDR.0000084083.71422.16 (2003).

23   Yung, A. *et al.* White matter volume and anisotropy in preterm children: a pilot study of neurocognitive correlates. *Pediatric research* **61**, 732-736, doi:10.1203/pdr.0b013e31805365db (2007).

24   Constable, R. T. *et al.* Prematurely born children demonstrate white matter microstructural differences at 12 years of age, relative to term control subjects: an investigation of group and gender effects. *Pediatrics* **121**, 306-316, doi:10.1542/peds.2007-0414 (2008).

25   Andrews, J. S. *et al.* Reading performance correlates with white-matter properties in preterm and term children. *Developmental medicine and child neurology* **52**, e94-100, doi:10.1111/j.1469-8749.2009.03456.x (2010).

26   Feldman, H. M. *et al.* White matter microstructure on diffusion tensor imaging is associated with conventional magnetic resonance imaging findings and cognitive function in adolescents born preterm. *Developmental medicine and child neurology* **54**, 809-814, doi:10.1111/j.1469-8749.2012.04378.x (2012).

27   Mullen, K. M. *et al.* Preterm birth results in alterations in neural connectivity at age 16 years. *Neuroimage* **54**, 2563-2570, doi:10.1016/j.neuroimage.2010.11.019 (2011).

28   Skranes, J. *et al.* Clinical findings and white matter abnormalities seen on diffusion tensor imaging in adolescents with very low birth weight. *Brain : a journal of neurology* **130**, 654-666, doi:10.1093/brain/awm001 (2007).

29   Vangberg, T. R. *et al.* Changes in white matter diffusion anisotropy in adolescents born prematurely. *Neuroimage* **32**, 1538-1548, doi:10.1016/j.neuroimage.2006.04.230 (2006).

30   Eikenes, L., Lohaugen, G. C., Brubakk, A. M., Skranes, J. & Haberg, A. K. Young adults born preterm with very low birth weight demonstrate widespread white matter alterations on brain DTI. *Neuroimage* **54**, 1774-1785, doi:10.1016/j.neuroimage.2010.10.037 (2011).

31   Allin, M. P. *et al.* White matter and cognition in adults who were born preterm. *PloS one* **6**, e24525, doi:10.1371/journal.pone.0024525 (2011).

32   Salvan, P. *et al.* Road work on memory lane--functional and structural alterations to the learning and memory circuit in adults born very preterm. *Neuroimage* **102 Pt 1**, 152-161, doi:10.1016/j.neuroimage.2013.12.031 (2014).

33   Kontis, D. *et al.* Diffusion tensor MRI of the corpus callosum and cognitive function in adults born preterm. *Neuroreport* **20**, 424-428, doi:10.1097/WNR.0b013e328325a8f9 (2009).

Reference

34   Ball, G. *et al.* The influence of preterm birth on the developing thalamocortical connectome. *Cortex; a journal devoted to the study of the nervous system and behavior* **49**, 1711-1721, doi:10.1016/j.cortex.2012.07.006 (2013).

35   Grothe, M. J. *et al.* Reduced Cholinergic Basal Forebrain Integrity Links Neonatal Complications and Adult Cognitive Deficits After Premature Birth. *Biol Psychiatry* **82**, 119-126, doi:10.1016/j.biopsych.2016.12.008 (2017).

36   Karolis, V. R. *et al.* Volumetric grey matter alterations in adolescents and adults born very preterm suggest accelerated brain maturation. *Neuroimage* **163**, 379-389, doi:10.1016/j.neuroimage.2017.09.039 (2017).

37   Meng, C. *et al.* Extensive and interrelated subcortical white and gray matter alterations in preterm-born adults. *Brain structure & function*, doi:10.1007/s00429-015-1032-9 (2015).

38   Nosarti, C. *et al.* Grey and white matter distribution in very preterm adolescents mediates neurodevelopmental outcome. *Brain : a journal of neurology* **131**, 205-217, doi:10.1093/brain/awm282 (2008).

39   Pierson, C. R. *et al.* Gray matter injury associated with periventricular leukomalacia in the premature infant. *Acta neuropathologica* **114**, 619-631, doi:10.1007/s00401-007-0295-5 (2007).

40   Lee, M. H., Smyser, C. D. & Shimony, J. S. Resting state fMRI: a review of methods and clinical applications. *AJNR. American journal of neuroradiology* **34**, 1866-1872, doi:10.3174/ajnr.A3263 (2013).

41   Lang, S., Duncan, N. & Northoff, G. Resting-state functional magnetic resonance imaging: review of neurosurgical applications. *Neurosurgery* **74**, 453-464; discussion 464-455, doi:10.1227/NEU.0000000000000307 (2014).

42   Ma, Y. *et al.* Resting-state hemodynamics are spatiotemporally coupled to synchronized and symmetric neural activity in excitatory neurons. *Proceedings of the National Academy of Sciences of the United States of America* **113**, E8463-E8471, doi:10.1073/pnas.1525369113 (2016).

43   Mateo, C., Knutsen, P. M., Tsai, P. S., Shih, A. Y. & Kleinfeld, D. Entrainment of Arteriole Vasomotor Fluctuations by Neural Activity Is a Basis of Blood-Oxygenation-Level-Dependent "Resting-State" Connectivity. *Neuron* **96**, 936-948 e933, doi:10.1016/j.neuron.2017.10.012 (2017).

44   Matsui, T., Murakami, T. & Ohki, K. Transient neuronal coactivations embedded in globally propagating waves underlie resting-state functional connectivity. *Proceedings of the National Academy of Sciences* **113**, 6556-6561, doi:10.1073/pnas.1521299113 (2016).

45   Schwalm, M. *et al.* Cortex-wide BOLD fMRI activity reflects locally-recorded slow oscillation-associated calcium waves. *eLife* **6**, e27602, doi:10.7554/eLife.27602 (2017).

46   Sanchez-Vives, M. V., Massimini, M. & Mattia, M. Shaping the Default Activity Pattern of the Cortical Network. *Neuron* **94**, 993-1001, doi:10.1016/j.neuron.2017.05.015 (2017).

47   Haynes, R. L., Sleeper, L. A., Volpe, J. J. & Kinney, H. C. Neuropathologic studies of the encephalopathy of prematurity in the late preterm infant. *Clinics in perinatology* **40**, 707-722, doi:10.1016/j.clp.2013.07.003 (2013).

48   Fransson, P. *et al.* Resting-state networks in the infant brain. *Proceedings of the National Academy of Sciences of the United States of America* **104**, 15531-15536, doi:10.1073/pnas.0704380104 (2007).

49   Smyser, C. D. *et al.* Longitudinal analysis of neural network development in preterm infants. *Cereb Cortex* **20**, 2852-2862, doi:10.1093/cercor/bhq035 (2010).

Reference

50   Smyser, C. D. *et al.* Resting-State Network Complexity and Magnitude Are Reduced in Prematurely Born Infants. *Cereb Cortex*, doi:10.1093/cercor/bhu251 (2014).

51   Smith-Collins, A. P., Luyt, K., Heep, A. & Kauppinen, R. A. High frequency functional brain networks in neonates revealed by rapid acquisition resting state fMRI. *Human brain mapping* **36**, 2483-2494, doi:10.1002/hbm.22786 (2015).

52   Smyser, C. D. *et al.* Effects of white matter injury on resting state fMRI measures in prematurely born infants. (2013).

53   White, T. P. *et al.* Dysconnectivity of neurocognitive networks at rest in very-preterm born adults. *NeuroImage. Clinical* **4**, 352-365, doi:10.1016/j.nicl.2014.01.005 (2014).

54   Degnan, A. J. *et al.* Altered Structural and Functional Connectivity in Late Preterm Preadolescence: An Anatomic Seed-Based Study of Resting State Networks Related to the Posteromedial and Lateral Parietal Cortex. *PloS one* **10**, e0130686, doi:10.1371/journal.pone.0130686 (2015).

55   Damaraju, E. *et al.* Resting-state functional connectivity differences in premature children. *Frontiers in systems neuroscience* **4**, doi:10.3389/fnsys.2010.00023 (2010).

56   Lubsen, J. *et al.* Microstructural and Functional Connectivity in the Developing Preterm Brain. *Seminars in Perinatology* **35**, 34-43, doi:10.1053/j.semperi.2010.10.006 (2011).

57   Finke, K. *et al.* Visual attention in preterm born adults: Specifically impaired attentional sub-mechanisms that link with altered intrinsic brain networks in a compensation-like mode. *Neuroimage* **107C**, 95-106, doi:10.1016/j.neuroimage.2014.11.062 (2015).

58   Bauml, J. G. *et al.* Correspondence Between Aberrant Intrinsic Network Connectivity and Gray-Matter Volume in the Ventral Brain of Preterm Born Adults. *Cereb Cortex*, doi:10.1093/cercor/bhu133 (2014).

59   Wilke, M., Hauser, T. K., Krageloh-Mann, I. & Lidzba, K. Specific impairment of functional connectivity between language regions in former early preterms. *Human brain mapping* **35**, 3372-3384, doi:10.1002/hbm.22408 (2014).

60   Scheinost, D. *et al.* The intrinsic connectivity distribution: a novel contrast measure reflecting voxel level functional connectivity. *Neuroimage* **62**, 1510-1519, doi:10.1016/j.neuroimage.2012.05.073 (2012).

61   Constable, R. T. *et al.* A left cerebellar pathway mediates language in prematurely-born young adults. *Neuroimage* **64**, 371-378, doi:10.1016/j.neuroimage.2012.09.008 (2013).

62   Scheinost, D. *et al.* Cerebral Lateralization is Protective in the Very Prematurely Born. *Cereb Cortex* **25**, 1858-1866, doi:10.1093/cercor/bht430 (2015).

63   Back, S. A. & Miller, S. P. Brain injury in premature neonates: A primary cerebral dysmaturation disorder? *Annals of neurology* **75**, 469-486, doi:10.1002/ana.24132 (2014).

64   Nosarti, C. *et al.* Preterm birth and structural brain alterations in early adulthood. *NeuroImage. Clinical* **6**, 180-191, doi:10.1016/j.nicl.2014.08.005 (2014).

65   Botellero, V. L. *et al.* Mental health and cerebellar volume during adolescence in very-low-birth-weight infants: a longitudinal study. *Child and adolescent psychiatry and mental health* **10**, 6, doi:10.1186/s13034-016-0093-8 (2016).

66   Botellero, V. L. *et al.* A longitudinal study of associations between psychiatric symptoms and disorders and cerebral gray matter volumes in adolescents born very preterm. *BMC pediatrics* **17**, doi:10.1186/s12887-017-0793-0 (2017).

67   de Kieviet, J. F., Zoetebier, L., van Elburg, R. M., Vermeulen, R. J. & Oosterlaan, J. Brain development of very preterm and very low-birthweight children in childhood

and adolescence: a meta-analysis. *Developmental medicine and child neurology* **54**, 313-323, doi:10.1111/j.1469-8749.2011.04216.x (2012).

68   Qiu, A., Mori, S. & Miller, M. I. Diffusion tensor imaging for understanding brain development in early life. *Annu Rev Psychol* **66**, 853-876, doi:10.1146/annurev-psych-010814-015340 (2015).

69   Doron, K. W. & Gazzaniga, M. S. Neuroimaging techniques offer new perspectives on callosal transfer and interhemispheric communication. *Cortex; a journal devoted to the study of the nervous system and behavior* **44**, 1023-1029, doi:10.1016/j.cortex.2008.03.007 (2008).

70   Glickstein, M. & Berlucchi, G. Classical disconnection studies of the corpus callosum. *Cortex; a journal devoted to the study of the nervous system and behavior* **44**, 914-927, doi:10.1016/j.cortex.2008.04.001 (2008).

71   McLaughlin, N. C. *et al.* Diffusion tensor imaging of the corpus callosum: a cross-sectional study across the lifespan. *International journal of developmental neuroscience : the official journal of the International Society for Developmental Neuroscience* **25**, 215-221, doi:10.1016/j.ijdevneu.2007.03.008 (2007).

72   Melhem, E. R. *et al.* Diffusion tensor MR imaging of the brain and white matter tractography. *AJR. American journal of roentgenology* **178**, 3-16, doi:10.2214/ajr.178.1.1780003 (2002).

73   Werring, D. *et al.* Diffusion tensor imaging can detect and quantify corticospinal tract degeneration after stroke. *Journal of neurology, neurosurgery, and psychiatry* **69**, 269-272, doi:10.1136/jnnp.69.2.269 (2000).

74   Drobyshevsky, A. *et al.* Developmental changes in diffusion anisotropy coincide with immature oligodendrocyte progression and maturation of compound action potential. *The Journal of neuroscience : the official journal of the Society for Neuroscience* **25**, 5988-5997, doi:10.1523/JNEUROSCI.4983-04.2005 (2005).

75   Shang, J. *et al.* Decreased BOLD fluctuations in lateral temporal cortices of premature born adults. *Human brain mapping*, doi:10.1002/hbm.24332 (2018).

76   Biswal, B. B. *et al.* Toward discovery science of human brain function. *Proceedings of the National Academy of Sciences of the United States of America* **107**, 4734-4739, doi:10.1073/pnas.0911855107 (2010).

77   Froudist-Walsh, S. *et al.* The effect of perinatal brain injury on dopaminergic function and hippocampal volume in adult life. *eLife* **6**, e29088, doi:10.7554/eLife.29088 (2017).

78   Baldoli, C. *et al.* Maturation of preterm newborn brains: a fMRI-DTI study of auditory processing of linguistic stimuli and white matter development. *Brain structure & function* **220**, 3733-3751, doi:10.1007/s00429-014-0887-5 (2015).

79   Zang, Y. F. *et al.* Altered baseline brain activity in children with ADHD revealed by resting-state functional MRI. *Brain & development* **29**, 83-91, doi:10.1016/j.braindev.2006.07.002 (2007).

80   Wang, Z. *et al.* Spatial patterns of intrinsic brain activity in mild cognitive impairment and Alzheimer's disease: a resting-state functional MRI study. *Human brain mapping* **32**, 1720-1740, doi:10.1002/hbm.21140 (2011).

81   Kannurpatti, S. S. & Biswal, B. B. Detection and scaling of task-induced fMRI-BOLD response using resting state fluctuations. *Neuroimage* **40**, 1567-1574, doi:10.1016/j.neuroimage.2007.09.040 (2008).

82   Zuo, X. N. *et al.* The oscillating brain: complex and reliable. *Neuroimage* **49**, 1432-1445, doi:10.1016/j.neuroimage.2009.09.037 (2010).

83   Bijsterbosch, J. *et al.* Investigations into within- and between-subject resting-state amplitude variations. *Neuroimage* **159**, 57-69, doi:10.1016/j.neuroimage.2017.07.014 (2017).

Reference

84   Raichle, M. E. The restless brain. *Brain connectivity* **1**, 3-12,
        doi:10.1089/brain.2011.0019 (2011).
85   Schwalm, M. *et al.* Cortex-wide BOLD fMRI activity reflects locally-recorded slow
        oscillation-associated calcium waves. *Elife* **6**, doi:10.7554/eLife.27602 (2017).
86   Neske, G. T. The Slow Oscillation in Cortical and Thalamic Networks: Mechanisms
        and Functions. *Frontiers in neural circuits* **9**, 88, doi:10.3389/fncir.2015.00088 (2015).
87   Ashburner, J. & Friston, K. J. Voxel-based morphometry--the methods. *Neuroimage*
        11, 805-821, doi:10.1006/nimg.2000.0582 (2000).
88   Pereira, F., Mitchell, T. & Botvinick, M. Machine learning classifiers and fMRI: a
        tutorial overview. *Neuroimage* **45**, S199-209, doi:10.1016/j.neuroimage.2008.11.007
        (2009).
89   de Wit, S. *et al.* Individual prediction of long-term outcome in adolescents at ultra-
        high risk for psychosis: Applying machine learning techniques to brain imaging data.
        Human brain mapping **38**, 704-714, doi:10.1002/hbm.23410 (2017).
90   Koutsouleris, N. *et al.* Detecting the psychosis prodrome across high-risk populations
        using neuroanatomical biomarkers. *Schizophr Bull* **41**, 471-482,
        doi:10.1093/schbul/sbu078 (2015).
91   Dwyer, D. B. *et al.* Brain Subtyping Enhances The Neuroanatomical Discrimination of
        Schizophrenia. *Schizophr Bull*, doi:10.1093/schbul/sby008 (2018).
92   Rozycki, M. *et al.* Multisite Machine Learning Analysis Provides a Robust Structural
        Imaging Signature of Schizophrenia Detectable Across Diverse Patient Populations
        and Within Individuals. *Schizophrenia Bulletin*, sbx137-sbx137,
        doi:10.1093/schbul/sbx137 (2017).
93   Koutsouleris, N. *et al.* Predicting Response to Repetitive Transcranial Magnetic
        Stimulation in Patients With Schizophrenia Using Structural Magnetic Resonance
        Imaging: A Multisite Machine Learning Analysis. *Schizophrenia Bulletin* (2017).
94   Mikolas, P. *et al.* Connectivity of the anterior insula differentiates participants with
        first-episode schizophrenia spectrum disorders from controls: a machine-learning
        study. *Psychological Medicine* **46**, 2695-2704, doi:10.1017/s0033291716000878
        (2016).
95   Cabral, C. *et al.* Classifying Schizophrenia Using Multimodal Multivariate Pattern
        Recognition Analysis: Evaluating the Impact of Individual Clinical Profiles on the
        Neurodiagnostic Performance. *Schizophr Bull* **42 Suppl 1**, S110-117,
        doi:10.1093/schbul/sbw053 (2016).
96   Greenstein, D., Malley, J. D., Weisinger, B., Clasen, L. & Gogtay, N. Using Multivariate
        Machine Learning Methods and Structural MRI to Classify Childhood Onset
        Schizophrenia and Healthy Controls. *Frontiers in Psychiatry* **3**,
        doi:10.3389/fpsyt.2012.00053 (2012).
97   Vogel, J. W. *et al.* Brain properties predict proximity to symptom onset in sporadic
        Alzheimer's disease. *Brain : a journal of neurology*, doi:10.1093/brain/awy093
        (2018).
98   Teipel, S. J. *et al.* Robust Detection of Impaired Resting State Functional Connectivity
        Networks in Alzheimer's Disease Using Elastic Net Regularized Regression. *Frontiers
        in aging neuroscience* **8**, 318, doi:10.3389/fnagi.2016.00318 (2016).
99   Smyser, C. D. *et al.* Prediction of brain maturity in infants using machine-learning
        algorithms. *Neuroimage* **136**, 1-9, doi:10.1016/j.neuroimage.2016.05.029 (2016).
100   Ball, G. *et al.* Machine-learning to characterise neonatal functional connectivity in
        the preterm brain. *Neuroimage* **124**, 267-275,
        doi:10.1016/j.neuroimage.2015.08.055 (2016).
101   Liem, F. *et al.* Predicting brain-age from multimodal imaging data captures cognitive
        impairment. *NeuroImage* (2016).

Reference

102   Cole, J. H., Leech, R., Sharp, D. J. & Alzheimer's Disease Neuroimaging, I. Prediction of brain age suggests accelerated atrophy after traumatic brain injury. *Annals of neurology* **77**, 571-581, doi:10.1002/ana.24367 (2015).

103   Koutsouleris, N. *et al.* Accelerated brain aging in schizophrenia and beyond: a neuroanatomical marker of psychiatric disorders. *Schizophr Bull* **40**, 1140-1153, doi:10.1093/schbul/sbt142 (2014).

104   Franke, K., Luders, E., May, A., Wilke, M. & Gaser, C. Brain maturation: predicting individual BrainAGE in children and adolescents using structural MRI. *Neuroimage* **63**, 1305-1312, doi:10.1016/j.neuroimage.2012.08.001 (2012).

105   Nosarti, C. Structural and functional brain correlates of behavioral outcomes during adolescence. *Early human development* **89**, 221-227 (2013).

106   Riegel, K., Orth, B., Wolke, D. & Osterlund, K. Die Entwicklung gefährdet geborener Kinder bis zum 5 Lebensjahr. Stuttgart,Germany: Thieme., doi:10.1093/cercor/bhn256 (1995).

107   Wolke, D. & Meyer, R. Cognitive status, language attainment, and prereading skills of 6-year-old very preterm children and their peers: the Bavarian Longitudinal Study. *Developmental Medicine & Child Neurology* **41**, 94-109 (1999).

108   Breeman, L. D., Jaekel, J., Baumann, N., Bartmann, P. & Wolke, D. Preterm Cognitive Function Into Adulthood. *Pediatrics* **136**, 415-423, doi:10.1542/peds.2015-0608 (2015).

109   Dubowitz, L. M., Dubowitz, V. & Goldberg, C. Clinical assessment of gestational age in the newborn infant. *The Journal of pediatrics* **77**, 1-10 (1970).

110   Prechtl, H. Neurological sequelae of prenatal and perinatal complications. *BMJ* **4**, 763-767 (1967).

111   Gutbrod, T., Wolke, D., Soehne, B., Ohrt, B. & Riegel, K. Effects of gestation and birth weight on the growth and development of very low birthweight small for gestational age infants: a matched group comparison. *Archives of Disease in Childhood - Fetal and Neonatal Edition* **82**, F208-F214, doi:10.1136/fn.82.3.F208 (2000).

112   von Aster, M., Neubauer, A. & Horn, R. Wechsler Intelligenztest für Erwachsene WIE. *Deutschsprachige Bearbeitung und Adaptation des WAIS-III von David Wechsler (2., korrigierte Auflage). Frankfurt: Pearson Assessment* (2006).

113   Chao-Gan, Y. & Yu-Feng, Z. DPARSF: A MATLAB Toolbox for "Pipeline" Data Analysis of Resting-State fMRI. *Frontiers in systems neuroscience* **4**, 13, doi:10.3389/fnsys.2010.00013 (2010).

114   Ashburner, J. & Friston, K. J. Unified segmentation. *Neuroimage* **26**, 839-851, doi:10.1016/j.neuroimage.2005.02.018 (2005).

115   Murphy, K., Bodurka, J. & Bandettini, P. A. How long to scan? The relationship between fMRI temporal signal to noise ratio and necessary scan duration. *Neuroimage* **34**, 565-574, doi:10.1016/j.neuroimage.2006.09.032 (2007).

116   Van Dijk, K. R., Sabuncu, M. R. & Buckner, R. L. The influence of head motion on intrinsic functional connectivity MRI. *Neuroimage* **59**, 431-438, doi:10.1016/j.neuroimage.2011.07.044 (2012).

117   Power, J. D., Barnes, K. A., Snyder, A. Z., Schlaggar, B. L. & Petersen, S. E. Spurious but systematic correlations in functional connectivity MRI networks arise from subject motion. *Neuroimage* **59**, 2142-2154, doi:10.1016/j.neuroimage.2011.10.018 (2012).

118   Chen, X. *et al.* Topological analyses of functional connectomics: A crucial role of global signal removal, brain parcellation, and null models. *Human brain mapping* **39**, 4545-4564, doi:10.1002/hbm.24305 (2018).

119   Power, J. D., Schlaggar, B. L. & Petersen, S. E. Recent progress and outstanding issues in motion correction in resting state fMRI. *Neuroimage* **105**, 536-551, doi:10.1016/j.neuroimage.2014.10.044 (2015).

120   Yan, C. G. *et al.* A comprehensive assessment of regional variation in the impact of head micromovements on functional connectomics. *Neuroimage* **76**, 183-201, doi:10.1016/j.neuroimage.2013.03.004 (2013).

121   Babu, P. & Stoica, P. Spectral analysis of nonuniformly sampled data – a review. *Digital Signal Processing* **20**, 359-378, doi:10.1016/j.dsp.2009.06.019 (2010).

122   Oakes, T. R. *et al.* Integrating VBM into the General Linear Model with voxelwise anatomical covariates. *Neuroimage* **34**, 500-508, doi:10.1016/j.neuroimage.2006.10.007 (2007).

123   He, Y. *et al.* Regional coherence changes in the early stages of Alzheimer's disease: a combined structural and resting-state functional MRI study. *Neuroimage* **35**, 488-500, doi:10.1016/j.neuroimage.2006.11.042 (2007).

124   Hansen, L. K. *et al.* Generalizable Patterns in Neuroimaging: How Many Principal Components? *NeuroImage* **9**, 534-544, doi:https://doi.org/10.1006/nimg.1998.0425 (1999).

125   Filzmoser, P., Liebmann, B. & Varmuza, K. Repeated double cross validation. *Journal of Chemometrics* **23**, 160-171, doi:10.1002/cem.1225 (2009).

126   Polikar, R. Ensemble based systems in decision making. *IEEE Circuits and systems magazine* **6**, 21-45 (2006).

127   Koutsouleris, N. *et al.* Individualized differential diagnosis of schizophrenia and mood disorders using neuroanatomical biomarkers. *Brain : a journal of neurology* **138**, 2059-2073, doi:10.1093/brain/awv111 (2015).

128   Saeys, Y., Inza, I. & Larranaga, P. A review of feature selection techniques in bioinformatics. *Bioinformatics* **23**, 2507-2517, doi:10.1093/bioinformatics/btm344 (2007).

129   Jonsson, P. & Wohlin, C. in *Software Metrics, 2004. Proceedings. 10th International Symposium on*   108-118 (IEEE, 2004).

130   Ball, G. *et al.* Development of cortical microstructure in the preterm human brain. *Proceedings of the National Academy of Sciences of the United States of America* **110**, 9541-9546, doi:10.1073/pnas.1301652110 (2013).

131   Yu, R. *et al.* Frequency-specific alternations in the amplitude of low-frequency fluctuations in schizophrenia. *Human brain mapping* **35**, 627-637, doi:10.1002/hbm.22203 (2014).

132   Itahashi, T. *et al.* Alterations of local spontaneous brain activity and connectivity in adults with high-functioning autism spectrum disorder. *Molecular autism* **6**, 30, doi:10.1186/s13229-015-0026-z (2015).

133   Tang, Y. *et al.* Neural activity changes in unaffected children of patients with schizophrenia: A resting-state fMRI study. *Schizophrenia research* **168**, 360-365, doi:10.1016/j.schres.2015.07.025 (2015).

134   Vercammen, A., Knegtering, H., den Boer, J. A., Liemburg, E. J. & Aleman, A. Auditory hallucinations in schizophrenia are associated with reduced functional connectivity of the temporo-parietal area. *Biol Psychiatry* **67**, 912-918, doi:10.1016/j.biopsych.2009.11.017 (2010).

135   Lemola, S. *et al.* Effects of gestational age on brain volume and cognitive functions in generally healthy very preterm born children during school-age: A voxel-based morphometry study. *PloS one* **12**, e0183519, doi:10.1371/journal.pone.0183519 (2017).

Reference

136   Spencer, M. D. *et al.* Low birthweight and preterm birth in young people with special educational needs: a magnetic resonance imaging analysis. *BMC medicine* **6**, 1, doi:10.1186/1741-7015-6-1 (2008).

137   Soria-Pastor, S. *et al.* Decreased regional brain volume and cognitive impairment in preterm children at low risk. *Pediatrics* **124**, e1161-1170, doi:10.1542/peds.2009-0244 (2009).

138   Ball, G. *et al.* Thalamocortical Connectivity Predicts Cognition in Children Born Preterm. *Cereb Cortex* **25**, 4310-4318, doi:10.1093/cercor/bhu331 (2015).

139   Ball, G. *et al.* The effect of preterm birth on thalamic and cortical development. *Cereb Cortex* **22**, 1016-1024, doi:10.1093/cercor/bhr176 (2012).

140   Toulmin, H. *et al.* Specialization and integration of functional thalamocortical connectivity in the human infant. *Proceedings of the National Academy of Sciences of the United States of America*, doi:10.1073/pnas.1422638112 (2015).

141   Kesler, S. R. *et al.* Volumetric analysis of regional cerebral development in preterm children. *Pediatric neurology* **31**, 318-325, doi:10.1016/j.pediatrneurol.2004.06.008 (2004).

142   Zubiaurre-Elorza, L. *et al.* Gray matter volume decrements in preterm children with periventricular leukomalacia. *Pediatric research* **69**, 554-560, doi:10.1203/PDR.0b013e3182182366 (2011).

143   Kesler, S. R. *et al.* Brain volume reductions within multiple cognitive systems in male preterm children at age twelve. *The Journal of pediatrics* **152**, 513-520, 520 e511, doi:10.1016/j.jpeds.2007.08.009 (2008).

144   Lean, R. E., Melzer, T. R., Bora, S., Watts, R. & Woodward, L. J. Attention and Regional Gray Matter Development in Very Preterm Children at Age 12 Years. *Journal of the International Neuropsychological Society : JINS* **23**, 539-550, doi:10.1017/S1355617717000388 (2017).

145   Nagy, Z. *et al.* Structural correlates of preterm birth in the adolescent brain. *Pediatrics* **124**, e964-972, doi:10.1542/peds.2008-3801 (2009).

146   Corbett-Detig, J. *et al.* 3D global and regional patterns of human fetal subplate growth determined in utero. *Brain structure & function* **215**, 255-263, doi:10.1007/s00429-010-0286-5 (2011).

147   Arichi, T. *et al.* Development of BOLD signal hemodynamic responses in the human brain. *Neuroimage* **63**, 663-673, doi:10.1016/j.neuroimage.2012.06.054 (2012).

148   Arichi, T. *et al.* Localization of spontaneous bursting neuronal activity in the preterm human brain with simultaneous EEG-fMRI. *eLife* **6**, e27814, doi:10.7554/eLife.27814 (2017).

149   Sanchez-Vives, M. V. & McCormick, D. A. Cellular and network mechanisms of rhythmic recurrent activity in neocortex. *Nature neuroscience* **3**, 1027-1034, doi:10.1038/79848 (2000).

150   Markram, H. *et al.* Reconstruction and Simulation of Neocortical Microcircuitry. *Cell* **163**, 456-492, doi:10.1016/j.cell.2015.09.029 (2015).

151   Gozzo, Y. *et al.* Alterations in neural connectivity in preterm children at school age. *Neuroimage* **48**, 458-463, doi:10.1016/j.neuroimage.2009.06.046 (2009).

152   Schafer, R. J. *et al.* Alterations in functional connectivity for language in prematurely born adolescents. *Brain : a journal of neurology* **132**, 661-670, doi:10.1093/brain/awn353 (2009).

153   Northam, G. B. *et al.* Interhemispheric temporal lobe connectivity predicts language impairment in adolescents born preterm. *Brain : a journal of neurology* **135**, 3781-3798, doi:10.1093/brain/aws276 (2012).

154   Aeby, A. *et al.* Language development at 2 years is correlated to brain microstructure in the left superior temporal gyrus at term equivalent age: a diffusion

tensor imaging study. *Neuroimage* **78**, 145-151, doi:10.1016/j.neuroimage.2013.03.076 (2013).

155   Rakic, P. Prenatal genesis of connections subserving ocular dominance in the rhesus monkey. *Nature* **261**, 467-471 (1976).

156   McConnell, S., Ghosh, A. & Shatz, C. Subplate neurons pioneer the first axon pathway from the cerebral cortex. *Science* **245**, 978-982, doi:10.1126/science.2475909 (1989).

157   Kanold, P. O. & Luhmann, H. J. The subplate and early cortical circuits. *Annu Rev Neurosci* **33**, 23-48, doi:10.1146/annurev-neuro-060909-153244 (2010).

158   Loh, W. Y. *et al.* Neonatal basal ganglia and thalamic volumes: very preterm birth and 7-year neurodevelopmental outcomes. *Pediatric research* **82**, 970-978, doi:10.1038/pr.2017.161 (2017).

159   Ligam, P. *et al.* Thalamic damage in periventricular leukomalacia: novel pathologic observations relevant to cognitive deficits in survivors of prematurity. *Pediatric research* **65**, 524-529, doi:10.1203/PDR.0b013e3181998baf (2009).

160   Boardman, J. P. *et al.* Abnormal deep grey matter development following preterm birth detected using deformation-based morphometry. *Neuroimage* **32**, 70-78, doi:10.1016/j.neuroimage.2006.03.029 (2006).

161   Young, J. M. *et al.* Deep grey matter growth predicts neurodevelopmental outcomes in very preterm children. *Neuroimage* **111**, 360-368, doi:10.1016/j.neuroimage.2015.02.030 (2015).

162   Counsell, S. J. *et al.* Thalamo-cortical connectivity in children born preterm mapped using probabilistic magnetic resonance tractography. *Neuroimage* **34**, 896-904, doi:10.1016/j.neuroimage.2006.09.036 (2007).

163   Lax, I. D. *et al.* Neuroanatomical consequences of very preterm birth in middle childhood. *Brain structure & function* **218**, 575-585, doi:10.1007/s00429-012-0417-2 (2013).

164   Peterson, B. S., Vohr, B., Staib, L. H. & et al. REgional brain volume abnormalities and long-term cognitive outcome in preterm infants. *JAMA : the journal of the American Medical Association* **284**, 1939-1947, doi:10.1001/jama.284.15.1939 (2000).

165   Bjuland, K. J., Rimol, L. M., Lohaugen, G. C. & Skranes, J. Brain volumes and cognitive function in very-low-birth-weight (VLBW) young adults. *European journal of paediatric neurology : EJPN : official journal of the European Paediatric Neurology Society* **18**, 578-590, doi:10.1016/j.ejpn.2014.04.004 (2014).

166   Dubois, J. *et al.* The early development of brain white matter: a review of imaging studies in fetuses, newborns and infants. *Neuroscience* **276**, 48-71, doi:10.1016/j.neuroscience.2013.12.044 (2014).

167   Wan, C. Y., Wood, A. G., Chen, J., Wilson, S. J. & Reutens, D. C. The influence of preterm birth on structural alterations of the vision-deprived brain. *Cortex; a journal devoted to the study of the nervous system and behavior* **49**, 1100-1109, doi:10.1016/j.cortex.2012.03.013 (2013).

168   Giedd, J. N. *et al.* Brain development during childhood and adolescence: a longitudinal MRI study. *Nature neuroscience* **2**, 861, doi:10.1038/13158 (1999).

169   Sowell, E. R., Thompson, P. M., Tessner, K. D. & Toga, A. W. Mapping continued brain growth and gray matter density reduction in dorsal frontal cortex: Inverse relationships during postadolescent brain maturation. *The Journal of neuroscience : the official journal of the Society for Neuroscience* **21**, 8819-8829 (2001).

170   Lenroot, R. K. *et al.* Differences in genetic and environmental influences on the human cerebral cortex associated with development during childhood and adolescence. *Human brain mapping* **30**, 163-174, doi:10.1002/hbm.20494 (2009).

Reference

171   Lenroot, R. K. & Giedd, J. N. The changing impact of genes and environment on brain development during childhood and adolescence: initial findings from a neuroimaging study of pediatric twins. *Development and psychopathology* **20**, 1161-1175, doi:10.1017/S0954579408000552 (2008).

172   Shaw, P. *et al.* Neurodevelopmental trajectories of the human cerebral cortex. *The Journal of neuroscience : the official journal of the Society for Neuroscience* **28**, 3586-3594, doi:10.1523/JNEUROSCI.5309-07.2008 (2008).

173   Sowell, E. R., Thompson, P. M., Holmes, C. J., Jernigan, T. L. & Toga, A. W. In vivo evidence for post-adolescent brain maturation in frontal and striatal regions. *Nature neuroscience* **2**, 859-861, doi:10.1038/13154 (1999).

174   Wu, X. *et al.* Frequency of Spontaneous BOLD Signal Differences between Moderate and Late Preterm Newborns and Term Newborns. *Neurotoxicity research* **30**, 539-551, doi:10.1007/s12640-016-9642-4 (2016).

175   Deng, Z., Chandrasekaran, B., Wang, S. & Wong, P. C. Resting-state low-frequency fluctuations reflect individual differences in spoken language learning. *Cortex; a journal devoted to the study of the nervous system and behavior* **76**, 63-78, doi:10.1016/j.cortex.2015.11.020 (2016).

176   Takeuchi, H. *et al.* Degree centrality and fractional amplitude of low-frequency oscillations associated with Stroop interference. *Neuroimage* **119**, 197-209, doi:10.1016/j.neuroimage.2015.06.058 (2015).

177   Zhao, C. *et al.* Structural and functional brain abnormalities in schizophrenia: A cross-sectional study at different stages of the disease. *Progress in neuro-psychopharmacology & biological psychiatry* **83**, 27-32, doi:10.1016/j.pnpbp.2017.12.017 (2017).

178   Hare, S. M. *et al.* Modality-Dependent Impact of Hallucinations on Low-Frequency Fluctuations in Schizophrenia. *Schizophr Bull*, doi:10.1093/schbul/sbw093 (2016).

179   Meda, S. A. *et al.* Frequency-Specific Neural Signatures of Spontaneous Low-Frequency Resting State Fluctuations in Psychosis: Evidence From Bipolar-Schizophrenia Network on Intermediate Phenotypes (B-SNIP) Consortium. *Schizophr Bull* **41**, 1336-1348, doi:10.1093/schbul/sbv064 (2015).

180   Lui, S. *et al.* Resting-state brain function in schizophrenia and psychotic bipolar probands and their first-degree relatives. *Psychol Med* **45**, 97-108, doi:10.1017/S003329171400110X (2015).

181   Mascali, D. *et al.* Intrinsic patterns of coupling between correlation and amplitude of low-frequency fMRI fluctuations are disrupted in degenerative dementia mainly due to functional disconnection. *PloS one* **10**, e0120988, doi:10.1371/journal.pone.0120988 (2015).

182   Li, R. *et al.* Altered regional activity and inter-regional functional connectivity in psychogenic non-epileptic seizures. *Scientific reports* **5**, 11635, doi:10.1038/srep11635 (2015).

183   Li, F. *et al.* Intrinsic brain abnormalities in attention deficit hyperactivity disorder: a resting-state functional MR imaging study. *Radiology* **272**, 514-523, doi:10.1148/radiol.14131622 (2014).

184   Cai, Y., Wu, X., Su, Z., Shi, Y. & Gao, J. H. Functional thalamocortical connectivity development and alterations in preterm infants during the neonatal period. *Neuroscience* **356**, 22-34, doi:10.1016/j.neuroscience.2017.05.011 (2017).

185   Wheelock, M. D. *et al.* Altered functional network connectivity relates to motor development in children born very preterm. *Neuroimage* **183**, 574-583, doi:10.1016/j.neuroimage.2018.08.051 (2018).

Reference

186   Gimenez, M. *et al.* Correlations of thalamic reductions with verbal fluency impairment in those born prematurely. *Neuroreport* **17**, 463-466, doi:10.1097/01.wnr.0000209008.93846.24 (2006).

187   Ball, G. *et al.* Rich-club organization of the newborn human brain. *Proceedings of the National Academy of Sciences* **111**, 7456-7461 (2014).

188   Leisman, G., Braun-Benjamin, O. & Melillo, R. Cognitive-motor interactions of the basal ganglia in development. *Frontiers in systems neuroscience* **8**, 16, doi:10.3389/fnsys.2014.00016 (2014).

189   Marsden, C. D. What do the basal ganglia tell premotor cortical areas? *Ciba Foundation symposium* **132**, 282-300 (1987).

190   Nambu, A. A new dynamic model of the cortico-basal ganglia loop. **143**, 461-466, doi:10.1016/s0079-6123(03)43043-4 (2004).

191   Hüppi, P. S. *et al.* Microstructural Development of Human Newborn Cerebral White Matter Assessed in Vivo by Diffusion Tensor Magnetic Resonance Imaging. *Pediatric research* **44**, 584, doi:10.1203/00006450-199810000-00019 (1998).

9. Abbreviation

ALFF	amplitude of low frequency fluctuations
AUC	area under curve
BAC	Balanced Accuracy
BLS	Bavarian Longitudinal Study
BOLD	blood oxygen dependent level
BW	birth weight
COD	coefficient of determination
DNTI	duration of Neonatal Treatment Index
FC	functional connectivity
FD	frame-wise displacement
FN	false-negative
FP	false-positive
FPR	false-positive rate
FT	full-term
GA	gestation age
GMV	gray matter volume
Hospital	duration of hospitalization
INTI	Intensity of Neonatal Treatment (Morbidity) Index (inti1+inti2)
IQ	intelligence quotient
IQ$_G$	full-scale intelligence quotient
IQp	performance intelligence quotient
IQv	verbal intelligence quotient
MAE	mean absolute error
MNI	Montreal Neurological Institute
MRI	magnetic resonance imaging
MSE	mean squared error
MVPA	multivariate pattern recognition analysis
NPV	negative predictive value
OPTI (neonatal)	optimality score of neonatal conditions
PCA	principal component analysis
PPV	positive predictive value
PT	preterm
rs-fMRI	resting-state functional MRI
SES	socioeconomic status at birth
sMRI	Structural MRI
SNR	Signal-to-noise ratio
SPM	Statistical Parametric Mapping
SPSS	Statistical Package for the Social Sciences
STL	superior temporal lobe
SVC	support vector classification
SVR	support vector regression
SVM	support vector machine
TIV	total intracranial volume
TN	true-negative
TP	true-positive
tSNR	temporal signal-to-noise ratio
VBM	voxel based morphometry
VLBW	very low birth weight
VP	very preterm
VPM	voxel probability map

10 Appendix

10.1 List of Figures

Appendix

10.2 List of Tables

10.3 Publications

Parts of this work are subject of the following publication by Human Brain Mapping:

<u>Shang, J.,</u> Bauml, J.G., Koutsouleris, N., Daamen, M., Baumann, N., Zimmer, C., Bartmann, P., Boecker, H., Wolke, D., Sorg, C. (2018) <u>Decreased BOLD fluctuations in lateral temporal cortices of premature born adults. Human brain mapping.</u>

<u>Shang, J.,</u> Fisher, P., Bauml, J.G., Daamen, M., Baumann, N., Zimmer, C., Bartmann, P., Boecker, H., Wolke, D., Sorg, C., Koutsouleris, N., Dwyer, D.B. (2019) <u>A machine learning investigation of volumetric and functional MRI abnormalities in adults born preterm. Human brain mapping.</u>

In cooperation with Dr. Felix Brandl the following co-authorship was achieved during my PhD candidate period.

Brandl, F., Avram, M., Weise, B., <u>Shang, J.,</u> Simoes, B., Bertram, T., Hoffmann Ayala, D., Penzel, N., Gursel, D.A., Bauml, J., Wohlschlager, A.M., Vukadinovic, Z., Koutsouleris, N., Leucht, S., Sorg, C. (2018) <u>Specific Substantial Dysconnectivity in Schizophrenia: A Transdiagnostic Multimodal Meta-analysis of Resting-State Functional and Structural Magnetic Resonance Imaging Studies. Biol Psychiatry.</u>

10.4 Poster presentations

<u>26th European Congress of Psychiatry 3-6 March 2018, Nice, France</u>

Aberrant Ongoing Brain Activity After Premature Birth

J. Shang [1,2], J.G. Bäuml [2,3], N. Koutsouleris [1], P. Bartmann [4], D. Wolke [5], C. Sorg [2,3,6]

[1]Ludwig-Maximilians-University, Department of Psychiatry and Psychotherapy, Munich, Germany;

[2]Technische Universität München, TUM-NIC Neuroimaging Center, Munich, Germany;

[3]Technische Universität München, Department of Neuroradiology, Munich, Germany;

[4]University Hospital Bonn- Germany, Department of Neonatology, Bonn,Germany;

[5]University of Warwick, Department of Psychology, Coventry, United Kingdom;

[6]Technische Universität München, Department of Psychiatry, Munich, Germany.

Appendix

<u>6th Biennial Schizophrenia International Research Society Conference in Florence, Italy on 4-8 April 2018</u>

Classifying Schizophrenia by Patterns of BOLD Fluctuations Using

Multivariate Pattern Recognition Analysis

Jing Shang[1,4], Christian Sorg[1,2,3], Josef G. Bäuml[1,3], Joseph Kambeitz[4], Felix, Brandl[1,3], Nikolaos Koutsouleris[4]*

[1] TUM-NIC Neuroimaging Center,

[2] Department of Psychiatry, Klinikum rechts der Isar and,

[3] Department of Neuroradiology, Technische Universität München, München, Germany;

[4] Department of Psychiatry and Psychotherapy, Ludwig-Maximilian-University, Munich, Germany

11. Acknowledgments

First, I feel really grateful for my two supervisors, Prof. Nikolaos Koutsouleris, Department of Psychiatry and Psychotherapy, Ludwig-Maximilian-University, Munich, Germany, and Dr. Christian Sorg from Technische Universität München, München, Germany, who supervised me during my PhD period in the past four years. Then I appreciate much help from Dr. Josef Bauml, Dr. Domnic Dwyer and Dr. Felix Brandl for the papers cooperation and data analysis.

Furthermore, I thank all current and former members of the Bavarian Longitudinal Study Group who contributed to general study organization, recruitment, and data collection, management and subsequent analyses, including (in alphabetical order): Barbara Busch, Stephan Czeschka, Claudia Grünzinger, Christian Koch, Diana Kurze, Sonja Perk, Andrea Schreier, Antje Strasser, Julia Trummer, and Eva van Rossum. We are grateful to the staff of the Department of Neuroradiology in Munich and the Department of Radiology in Bonn for their help in data collection.